iScience

CellPress

Article

Semaphorin 6A–Plexin A2/A4 Interactions with Radial Glia Regulate Migration Termination of Superficial Layer Cortical Neurons

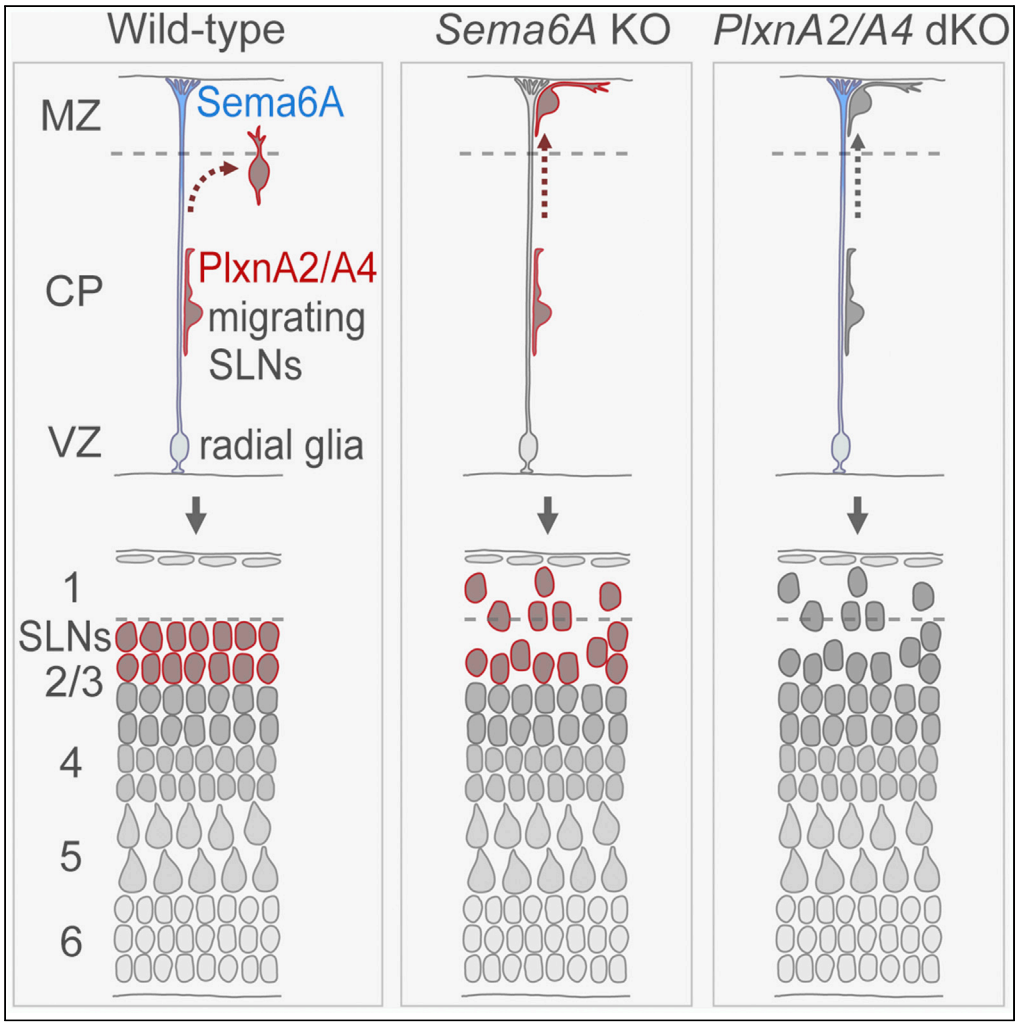

Yumiko Hatanaka, Takahiko Kawasaki, Takaya Abe, ..., Akira Sakakibara, Yasuo Kawaguchi, Tatsumi Hirata

yhatanaka-ns@umin.ac.jp

HIGHLIGHTS

Loss of PlxnA2/A4 results in superficial layer neurons invading layer 1

PlxnA2/A4 works cell autonomously to settle these neurons properly

Lack of Sema6A in radial glial cells causes similar mispositioning of these neurons

Sema6A–PlxnA2/A4 signaling determines settling position of superficial layer neurons

Hatanaka et al., iScience *21*, 359–374
November 22, 2019
https://doi.org/10.1016/j.isci.2019.10.034

iScience

CellPress

Article

Semaphorin 6A–Plexin A2/A4 Interactions with Radial Glia Regulate Migration Termination of Superficial Layer Cortical Neurons

Yumiko Hatanaka,[1,2,6,7,8,*] Takahiko Kawasaki,[3,7] Takaya Abe,[4] Go Shioi,[4] Takao Kohno,[5] Mitsuharu Hattori,[5] Akira Sakakibara,[6] Yasuo Kawaguchi,[2] and Tatsumi Hirata[3]

SUMMARY

Precise regulation of neuronal migration termination is crucial for the establishment of brain cytoarchitectures. However, little is known about how neurons terminate migration. Here we focused on interactions between migrating cortical neurons and their substrates, radial glial (RG) cells, and analyzed the role of Plexin A2 and A4 (PlxnA2/A4) receptors and their repulsive ligand, Semaphorin 6A (Sema6A), for this process. In both *PlxnA2/A4* double-knockout and *Sema6A* mutant mice, the outermost cortical plate neurons ectopically invade layer 1 at a stage when they should reach their destinations. PlxnA2/A4 proteins are abundantly expressed on their leading processes, whereas *Sema6A* mRNA is enriched in RG cell somata. Cell-targeted gene expression and conditional knockouts indicate critical roles for these molecules. We hypothesize that the timely appearance of repulsive signaling mediated by Sema6A–PlxnA2/A4 weakens migrating neuron–RG cell interactions, leading to migration termination.

INTRODUCTION

Neuronal migration is crucial for establishing a neuronal architecture with functional integrity. During development, newborn neurons migrate from progenitor zones toward their final destinations, where they form specific neuronal architectures and functional circuits. Disturbance of these migrations alters neuronal positioning, causing cytoarchitectonic abnormalities and consequent functional deficiencies (Barkovich et al., 2012, 2015; Moffat et al., 2015).

Neuronal migration has been extensively studied using the cerebral cortex. Cortical excitatory neurons, which are born in the cortical ventricular zone (VZ)/sub-VZ, migrate radially through the cortical plate (CP) along radial glial (RG) fibers. Although the RG fibers reach the pial surface spanning the marginal zone (MZ), the future layer 1 (L1), the migrating neurons terminate migration just beneath the MZ and establish a sharply demarcated laminar structure.

The process of neuronal migration can be divided into three steps: initiation, continuation, and termination. Although the cellular and molecular mechanisms for the first two steps have been relatively well studied (for reviews, see Evsyukova et al., 2013; Ohtaka-Maruyama and Okado, 2015; Sekine et al., 2013), our knowledge about the termination of migration is still limited.

Termination may be caused by the detachment of migrating cortical neurons from the RG fibers due to a weakening of adhesion between them at the top of the CP (Goffinet, 1984). Furthermore, increased neuron–neuron adhesion may override neuron–RG fiber adhesion at the top of the CP, thereby contributing to the detachment of neurons from the RG fibers (Goffinet, 1984). The observation that cortical neurons whose migration is terminating are more closely packed supports this notion (Goffinet, 1984; Sekine et al., 2014). However, whether active changes in the interaction between neurons and RG fibers are indeed required for terminal migration is unknown.

To date, several genes are known to affect migration termination. These include genes that disrupt the integrity of the pial basement membrane (BM) (Costa et al., 2001; Herms et al., 2004; Jeong et al., 2013; Moers et al., 2008; Nakagawa et al., 2015; Niewmierzycka et al., 2005), reelin (D'Arcangelo, 2005), reelin-related genes (Ha et al., 2017; Hack et al., 2007; Herrick and Cooper, 2002; Hirota et al., 2018; Kohno et al., 2015), and SPARC-like 1 (Gongidi et al., 2004).

[1]Graduate School of Frontier Biosciences, Osaka University, 1-3 Yamadaoka, Suita, Osaka 565-0871, Japan

[2]Division of Cerebral Circuitry, National Institute for Physiological Sciences, 5-1 Higashiyama, Myodaiji, Okazaki, Aichi 444-8787, Japan

[3]Brain Function Laboratory, National Institute of Genetics, 1111 Yata, Mishima, Shizuoka 411-8540, Japan

[4]Laboratory for Animal Resources and Genetic Engineering, RIKEN Center for Biosystems Dynamics Research, 2-2-3 Minatojima Minami-machi, Chuou-ku, Kobe, Hyogo 650-0047, Japan

[5]Department of Biomedical Science, Graduate School of Pharmaceutical Sciences, Nagoya City University, 3-1 Tanabe-dori, Mizuho-ku, Nagoya, Aichi 467-8603, Japan

[6]College of Life and Health Sciences, Chubu University, 1200 Matsumoto-cho, Kasugai, Aichi 487-8501, Japan

[7]These authors contributed equally to the experimental part of this study

[8]Lead Contact

*Correspondence: yhatanaka-ns@umin.ac.jp

https://doi.org/10.1016/j.isci.2019.10.034

Here we focused on Semaphorins (Semas) and their receptors. Semas are a large and diverse family of signaling proteins composed of secreted as well as transmembrane proteins and were originally identified as repulsive axonal guidance molecules in the nervous system (Goodman et al., 1999). Their receptors are mainly the Plexin (Plxn) family (Battistini and Tamagnone, 2016). Among Semas, the transmembrane-type Sema ligands Sema6A and 6B bind to the PlxnA subfamily members PlxnA2 and PlxnA4 (Suto et al., 2005; Toyofuku et al., 2008; Tawarayama et al., 2010). Their interactions regulate cell adhesion positively or negatively, depending on the situation, and contribute to the establishment of neural circuits such as corticospinal (Faulkner et al., 2008; Rünker et al., 2008) and thalamocortical projections (Leighton et al., 2001; Little et al., 2009; Mitsogiannis et al., 2017), laminar-restricted projections of hippocampal mossy fibers (Suto et al., 2005; Tawarayama et al., 2010), and laminar targeting of retinal neurons (Matsuoka et al., 2011). They also regulate cerebellar granule cell migration (Kerjan et al., 2005; Renaud et al., 2008) and interkinetic nuclear migration of retinal progenitor cells (Belle et al., 2016).

In this study, we show that a temporally regulated change in Sema6A–PlxnA2/A4 interaction between migrating neurons and RG cells is required for correct termination of neuronal migration. Superficial layer neurons (SLNs) located at the outermost part of layers 2 and 3 (L2/3) ectopically invade L1 in *PlxnA2/A4* double-knockout (KO) (dKO) mice as well as *Sema6A* KO mice. Anatomical and genetic analyses suggest that PlxnA2/A4 proteins on the migrating SLNs and Sema6A protein on the RG processes interact to suppress cell invasion into L1, probably by regulating the adhesiveness between SLNs and RG fibers.

RESULTS

Irregular Arrangement of SLNs in *PlxnA2/A4* dKO Cortex

PlxnA2 and A4 are widely expressed in mouse cerebral cortex during embryonic and perinatal stages (Murakami et al., 2001; Suto et al., 2003); although their roles have been studied in other systems, little is known about their contribution to cortical development. To explore their role, we first analyzed the cortical phenotype of *PlxnA2* and *A4* single- and double-mutant mice at P15.

In wild-type ($PlxnA2^{+/+}A4^{+/+}$), double-heterozygous ($PlxnA2^{+/-}A4^{+/-}$), or compound mutant mice carrying only a single wild-type allele for *PlxnA2* or *A4* ($PlxnA2^{-/-}A4^{+/-}$ and $PlxnA2^{+/-}A4^{-/-}$), the boundary between L1 and L2/3 was clearly demarcated by a difference in cell density (Figures 1A and S1A–S1C, wild-type, $n = 2$; $PlxnA2^{+/-}A4^{+/-}$, $n = 3$; $PlxnA2^{-/-}A4^{+/-}$, $n = 3$; $PlxnA2^{+/-}A4^{-/-}$, $n = 2$). In contrast, when both *PlxnA2* and *A4* were knocked out ($PlxnA2^{-/-}A4^{-/-}$; *PlxnA2/A4* dKO), the boundary became blurred and rippled and SLNs appeared to invade L1 (Figure 1B, $n = 3$). The mislocation of SLNs across the rostro-caudal axis tended to occur with a medial-low/lateral-high gradient. For example, the mislocation appeared to be more prominent in the lateral regions including the primary somatosensory (S1), auditory, and visual areas (not shown) than in the medial cortical regions that include the primary motor area (M1). In the lateral regions, neurons that invaded L1 sometimes formed clusters, giving rise to a ruffled L1–L2/3 border (Figure 1B, b2, $n = 3$). These observations indicate that PlxnA2 and A4 redundantly regulate correct neuronal positioning, leading to the formation of a sharp boundary between L1 and L2/3.

Excitatory SLNs Are Mislocated in L1 of *PlxnA2/A4* dKO Mice

We next attempted to determine the identity of malpositioned cells in the *PlxnA2/A4* dKO mice. At P15, cellular arrangements in the cortex appeared normal (Figures 2A and 2F: hereafter, double-heterozygous mice were used as a control unless otherwise noted). For example, small- and medium-sized neurons were located in L2–4, large-sized neurons in L5 at a low density, and medium-sized neurons in L6, in a manner similar to the control ($n = 3$). Expression of layer-specific neuronal markers also showed normal neuronal positioning in each layer (Figures 2B–2D, 2G–2I, and S2A–S2C). However, Wolframin protein (Wfs-1)-positive cells, which are normally located in the outer part of L2/3 (Luuk et al., 2008) (Figure 2E), were mislocated in L1 in the dKO mice (Figure 2J). Thus the vast majority of mislocated neurons were SLNs, but not other layer neurons.

In the dKO cortex, the numbers of lamina-specific neuronal marker-positive cells (Figure 2K) and cleaved caspase 3-positive cells (Figure S2F) were comparable with those in control, suggesting that neither cell type conversion nor cell death is responsible for the mislocalization phenotype. The mislocated SLNs may be mostly excitatory, because (1) they were positive for Cux1, which is expressed in pyramidal neurons, but not parvalbumin-positive inhibitory neurons (Nieto et al., 2004) (Figures 2L–2M″), and (2) the density of

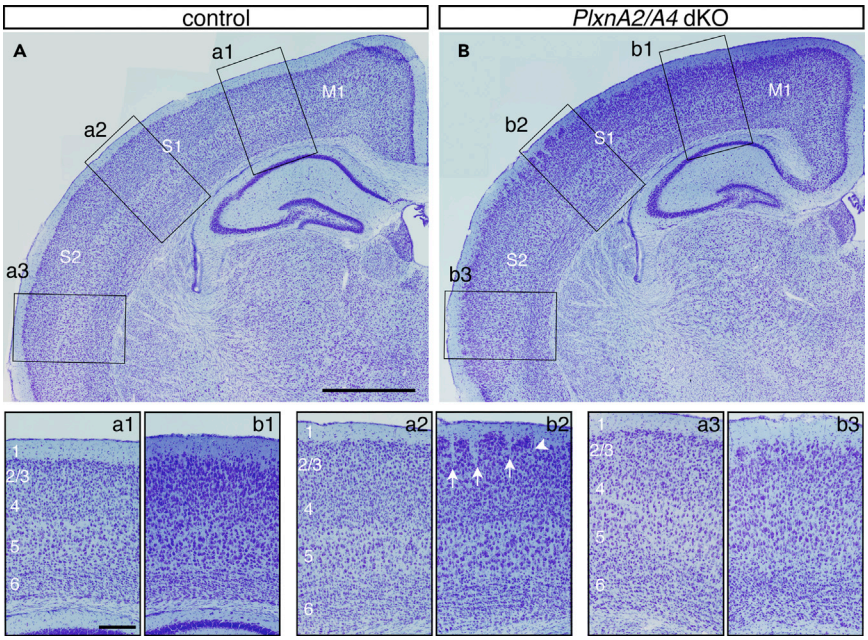

Figure 1. Cortical Cytoarchitecture of *PlxnA2/A4* dKO Mice

(A and B) Nissl staining of coronal sections from a *PlxnA2/A4* double heterozygote, as a control (A), and a dKO mouse (B) at P15. In the dKO mouse, SLNs, which are normally located in the outermost regions of L2/3, were dispersed into L1. M1, primary motor area; S1, primary somatosensory area; S2, secondary somatosensory area. Lower panels show higher-magnification views of dorsal (a1 and b1), dorsolateral (a2 and b2), and lateral (a3 and b3) regions of the sections in (A) and (B). In lateral regions of dKO mice, cells sometimes formed clusters as shown in b2; arrows and an arrowhead indicate vertical and horizontal gaps around clusters, respectively. The frequency of appearance of clusters varied among animals, but they tended to appear in a rostro-medial-low/caudo-lateral-high gradient manner. See also Figure S1. Scale bars: 1 mm in (A and B) and 200 μm in (a1–b3).

GABAergic inhibitory neurons in L1 and nearby appeared unchanged (Figures 2N–2O′). Together, these results indicated that excitatory SLNs showed aberrant distribution in *PlxnA2/A4* dKO mice.

Mislocation of SLNs Manifests during the Early Postnatal Stage

To determine the initial event that is primarily responsible for SLN mislocation, we examined the time at which the mislocation first appeared in the *PlxnA2/A4* dKO mice. We focused on the prospective S1 area, which at a later stage displayed a typical mislocation phenotype. Nissl staining patterns of dKO mice were indistinguishable from those of control mice at postnatal day (P)1, when cell-sparse L1 became identifiable (Figures 2P and 2Q); however, a few ectopic cells, which were positive for Satb2 (Satb2$^+$), a marker of upper layer neurons, had already appeared in L1 of the dKO mice at this stage (Figures 2P′ and 2Q′). At P3, the L1–L2/3 boundary became less clear (Figures 2R and 2S), largely due to spreading of Satb2$^+$ cells into L1 (Figures 2R′ and 2S′). The malpositioning of Satb2$^+$ cells tended to be more prominent in the lateral than in the medial cortex but these cells did not form clear clusters at this stage. By P7, the disorganized superficial layer structures in the dKO mice were readily recognizable by Nissl staining (Figures 2T–2U′). Thus the first indication of neuronal mislocation occurred at P1, and the mislocation became apparent at P3.

SLNs Appear to Overmigrate beyond the Normal Settling Position

The period of P1–P3 when the mislocated phenotype of neurons becomes apparent corresponds to the period when wild-type SLNs reach the top of the CP to terminate migration (Hatanaka et al., 2004). This suggests that the observed phenotype is a result of aberrant termination of neuronal migration. To explore this possibility, we carried out a birthdating study by injection of bromodeoxyuridine (BrdU) at embryonic day (E)15.5 or E16.5, stages when L2/3 neurons are born. Overall, the distribution of BrdU$^+$ cells was similar between control and dKO mice, indicating their normal migration from the VZ toward L2/3 (Figures 3A–3D). However, the mean cell position (Dm, see legend to Figure 3) was slightly higher in the dKO mice,

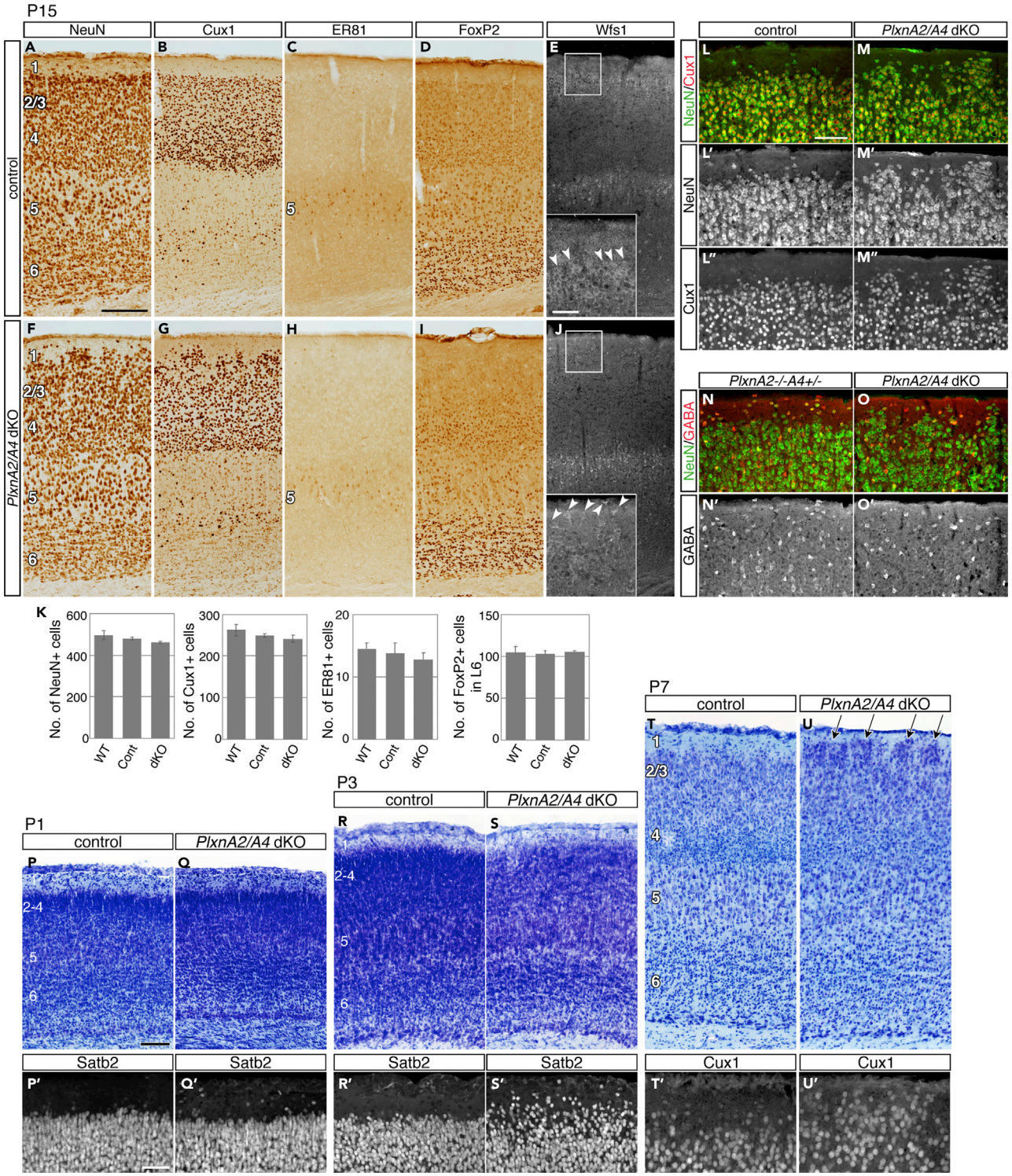

Figure 2. Mislocation of SLNs in *PlxnA2/A4* dKO Mice and Its Developmental Onset

(A–J) Immunostaining using cortical layer markers. Coronal sections from P15 control (A–E) and *PlxnA2/A4* dKO mouse (F–J). NeuN, pan-neuronal marker; Cux1, marker for L2–4 neurons; ER81, marker for L5 neurons; FoxP2, marker for L6 neurons; and Wfs1, marker for upper L2/3 and L5 neurons. Insets at the bottom of (E) and (J) are higher-magnification views of the L1–L2/3 regions indicated by rectangles. Arrowheads indicate Wfs1-positive cells.

Figure 2. *Continued*

(K) Bar histograms showing the number of marker-positive cells within a 100-μm-wide region of S1. Four 100-μm-wide regions within S1 were sampled for each genotype. Data are represented as mean ± SEM. No significant statistical difference was found for any combination of the data in the histogram (one-way ANOVA followed by Tukey's post-hoc test).

(L–M″) Immunostaining using anti-NeuN and Cux1. Mislocated neurons were mostly Cux1-positive.

(N–O′) Immunostaining using anti-NeuN and GABA. Distribution of $GABA^+$ cells appeared similar between control ($A2^{-/-}A4^{+/-}$) and dKO mice in the locations where ectopic neuronal distribution was evident.

(P–U′) Nissl staining of presumptive primary somatosensory area of control and dKO mice at P1, P3, and P7. (P′–U′) Immunostaining using anti-Satb2 or Cux1. Satb2 marks L2–6 callosal neurons that are excitatory (Britanova et al., 2008; Huang et al., 2013) and start to be expressed earlier than Cux1. By P7, ectopic cells sometimes formed clusters (arrows).

See also Figures S2 and S5. Scale bars: 200 μm in (A–J), 50 μm in insets of (E and J) and in (P′–U′), and 100 μm in (L–O′) and (P–U).

suggesting the occurrence of overmigration (Figure 3A′–3D′). To further explore this possibility, we labeled SLNs by *in utero* electroporation (IUE) at E15.5 and examined their morphology at P3. We found that a majority of GFP^+ cells had reached the top of the CP in both control and dKO mice (Figures 3E, 3E′, 3H, and 3H′). A close examination, however, revealed that whereas most GFP^+ cells were confined to the CP in control mice (Figures 3E and 3E′), a substantial proportion was dispersed into L1 of the dKO mice (Figures 3H and 3H′). In both control and dKO mice, GFP^+ cells typically extended their thick apical processes toward the pial surface (Figures 3F and 3G). However, apical processes in dKO mice tended to be shorter than those in the control mice (Figures 3I and 3J). Notably, some GFP^+ cells in close proximity to the pial surface extended a thick process pointing to the ventricle (Figure 3J). Together, these observations are consistent with the view that SLNs migrate beyond their normal settling position in *PlxnA2/A4* dKO mice.

Although breaches in the pial BM result in neuronal ectopias (Costa et al., 2001; Herms et al., 2004; Jeong et al., 2013; Moers et al., 2008; Nakagawa et al., 2015; Niewmierzycka et al., 2005), we found unaltered laminin expression in the dKO mice (Figure S2G), indicating that BM defects were not the cause of the phenotype observed here.

Overlapping Expression of PlxnA2 and A4 in Neurons at the Top of the CP

Both *PlxnA2* and *A4* mRNA showed developmental stage-dependent expression profiles from E15.5 through to P7 (Figures 4A–4H, Murakami et al., 2001; Suto et al., 2003). Importantly, at P0 and P3, both transcripts were abundant at the top of the CP (arrowheads), where SLNs should settle. We also found that both PlxnA2 and A4 proteins were enriched in L1 (Figures 4M–4N″). Within this layer, the site of high PlxnA2 and A4 immunoreactivities was found in close proximity to SLN leading processes (Figures 4O and 4P). These findings are consistent with the idea that the leading processes of SLNs express both PlxnA2 and A4 proteins.

Cell-Autonomous Function of PlxnA2

PlxnA2/A4 expression on SLNs raises the possibility that these molecules function cell autonomously in SLNs. We tested this by introducing *PlxnA2* (Figure S3A) into the *PlxnA2/A4* dKO mice at E15.5 by IUE. In wild-type (Figures S3B and S3C) and control mice (Figure 5A, see also Figure 3E), expression of *GFP* alone (*GFP*) or a mixture of *GFP* and *PlxnA2* (*GFP/Plxn2*), respectively, yielded virtually no GFP^+ or GFP/$PlxnA2^+$ cells in L1 (0% of total GFP/$PlxnA2^+$ cells above the white matter [WM], $n = 3$ brains, total 1,336 cells, control, Figure 5H; wild-type, data not shown). In contrast, in dKO mice transfected with *GFP*, a substantial fraction of GFP^+ cells were observed in L1 (32.6% ± 8.4%, $n = 3$ brains, total 1,923 cells, Figures 5B and 5H). Expression of Sab2 indicates that these were SLNs (Figure 5E). However, forced expression of *GFP/PlxnA2* rescued this phenotype, greatly reducing the number of GFP/$PlxnA2^+$ cells in L1 (8.1% ± 0.7%, $n = 3$ brains, total 2,012 cells, Figures 5C and 5H). Importantly, untransfected SLNs were still abundantly mislocated in L1 and there was no difference in the number of $GFP^-/Satb2^+$ cells between *GFP*- and *GFP/PlxnA2*-transfected animals (Figure 5G). Thus, these results indicate that PlxnA2 functions cell autonomously for proper SLN positioning.

Some GFP/$PlxnA2^+$ cells of the dKO mice appeared to prematurely halt migration beneath L1, exhibiting elaborated apical processes (Figure 5F). This may be because PlxnA2 started to be expressed in SLNs earlier than its endogenous expression under a strong constitutive promoter (Niwa et al., 1991). On closer examination, the elaborated apical processes were somewhat tangled, implying an additional effect of PlxnA2 expression. In extreme cases, GFP/PlxnA2-$high^+$ cells in the WM of the dKO mice showed prominent aggregation (Figure S3F).

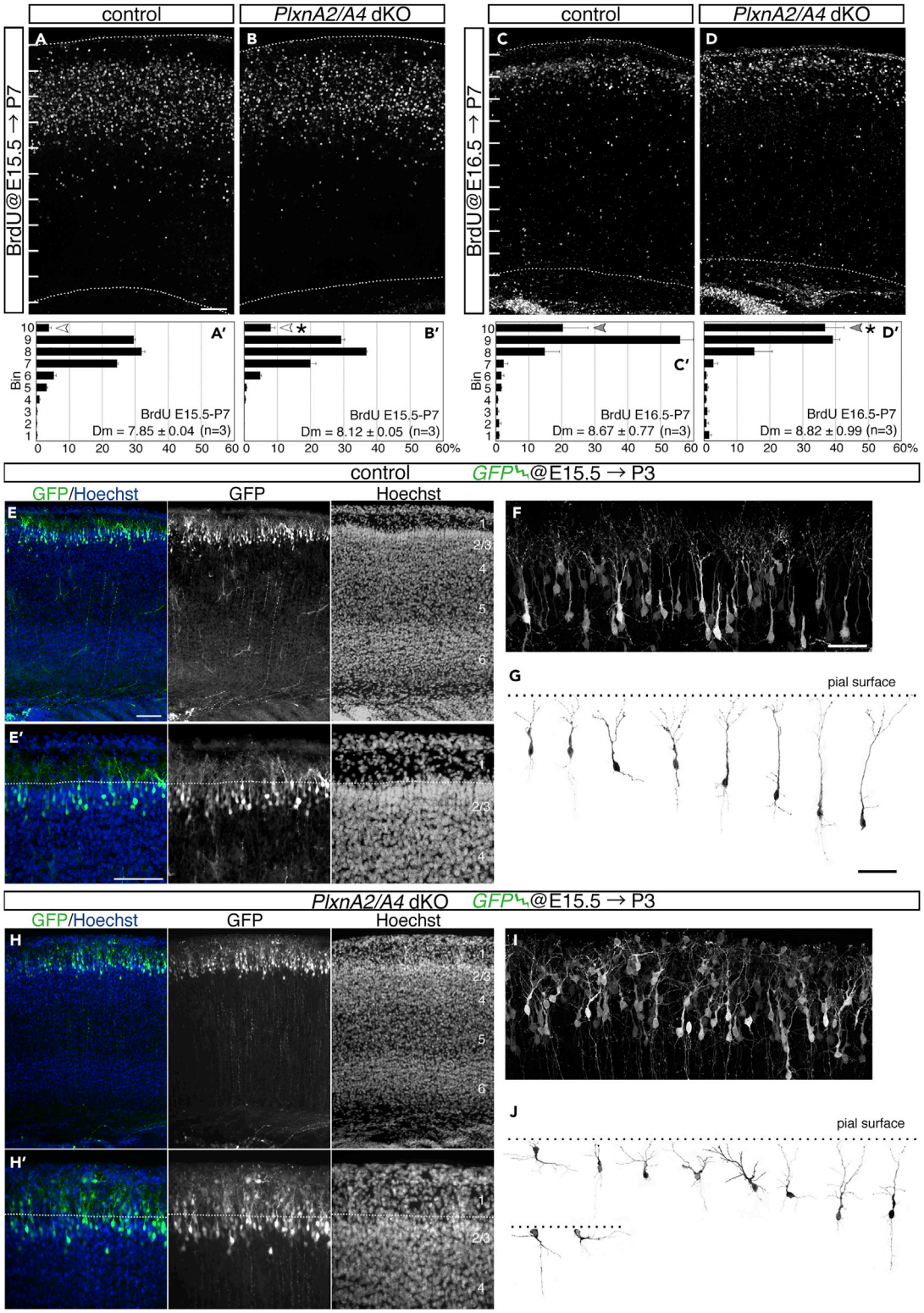

Figure 3. SLNs Are Ectopically Positioned in L1 of *PlxnA2/A4* dKO Mice

(A–D) Distribution of BrdU$^+$ cells. BrdU was injected at either E15.5 (A and B) or E16.5 (C and D), stages of neurogenesis for SLNs in mice (Smart and Smart, 1982). BrdU$^+$ cells were examined at P7. (A and C) Control and (B and D) *PlxnA2/A4* dKO mice. (A′–D′) Bar histograms showing laminar distribution of BrdU$^+$ cells. The cerebral wall was divided into 10 equal bins (bin 1–10) from the bottom of L6 to the pial surface, which is delineated by dotted lines in (A–D). Bins 10

Figure 3. *Continued*

and 9–7 approximately correspond to L1 and L2–4, respectively. The mean cell position (Dm) in each sample was calculated as Σ(NiDi)/Σ(Ni), where Ni is the number of $BrdU^+$ cells in bin Di. Data are represented as mean ± SEM. The Dm value of the dKO mouse was slightly higher, showing a significant difference for E15.5 ($p = 0.01$), but not E16.5, injection ($p = 0.22$); in both cases, the proportion of cells in bin 1 was significantly higher in the dKO mouse. *$p < 0.05$ (Student's t test).

(E–J) Location and morphology of SLNs at the stage of migration termination. GFP^+ SLNs of control mice were localized to the uppermost regions of L2/3 (E and E′), whereas those of *PlxnA2/A4* dkO mice were additionally found in L1 (H and H′). The dotted line in (E′) and (H′) indicates the position of the L1–L2/3 boundary. (F and I) Higher-magnification views, and (G and J) 3D reconstruction images of GFP^+ SLNs. The dotted line indicates the position of the pial surface.

See also Figure S5. Scale bars: 100 μm in (A–D), (E and H) and (E′ and H′), and 50 μm in (F and I) and (G and J).

Mutation of *Sema6A* Phenocopies the *PlxnA2/A4* dKO Phenotype

PlxnA2 and A4 are the receptors for the transmembrane Semas, Sema6A and 6B. Although both Sema6s bind to PlxnA2 and A4 (Suto et al., 2005; Toyofuku et al., 2008; Tawarayama et al., 2010), the binding affinity of Sema6B to PlxnA2 is relatively low (Tawarayama et al., 2010). To identify the Semas involved in proper SLN positioning, we first examined two different mutant alleles for *Sema6A*, *Sema6A* gene trap (*Sema6A*$^{-/-}$, Rünker et al., 2011) and *Sema6A* exon 3 deletion (*Sema6A*$^{\Delta/\Delta}$, Figure S4), and found that both homozygotes showed a disrupted L1–L2/3 boundary (*Sema6A*$^{-/-}$ at P15, $n = 2$ brains, Figure 6A and Rünker et al., 2011; *Sema6A*$^{\Delta/\Delta}$ at P3, $n = 6$ brains, Figure 6C), similar to the *PlxnA2/A4* dKO cortex. Quantitatively, we found no significant changes in the number of cortical neurons between control and *Sema6A*$^{\Delta/\Delta}$ mice (Figures S2D and S2E), as was the case for control and *PlxnA2/A4* dKO mice (Figures S2C and S2E). Moreover, SLN mislocation became manifest around P3 (*Sema6A*$^{\Delta/\Delta}$, Figure S5A) and was most severe in the lateral region, showing a medial-low/lateral-high gradient. Immunohistochemical examination indicated that their BM structure, similar to *PlxnA2/A4* dKO mice, was normal (data not shown). To corroborate these findings, we used the same IUE protocol that was applied for *PlxnA2/A4* dKO mice. We labeled SLNs by IUE with *GFP* at E15.5 and examined GFP^+ neurons at P3. Of the labeled cells in the CP and L1, the proportion of those in L1 in *Sema6A*$^{\Delta/\Delta}$ mice was comparable to that in *PlxnA2/A4* dKO mice (Figures 5D and 5H, 33.2 ± 3.11%, $n = 2$ brains). Furthermore, the morphologies of these cells resembled those in *PlxnA2/A4* dKO mice (Figure S5B, see also Figure 3). Unlike in *Sema6A*$^{\Delta/\Delta}$ mice, we found no ectopic SLNs in L1 of the *Sema6A*$^{+/-}$*Sema6B*$^{-/-}$ compound mutant mice ($n = 2$ brains; Figure 6B), indicating the importance of *Sema6A*. In addition, when *PlxnA2* was electroporated into *Sema6A*$^{\Delta/\Delta}$ mice, SLN mislocation was hardly rescued (Figure S5C). Taking these observations together, it is highly likely that Sema6A is the PlxnA2/A4 ligand involved in proper positioning of SLNs.

The Source of Sema6A for Interaction with PlxnA2/A4 in L1

We next examined the distribution of *Sema6A* transcript during the perinatal period to identify the source of Sema6A that interacts with PlxnA2/A4. *Sema6A* mRNA was sparsely expressed throughout the cerebral cortex, but was prominent in the VZ from P0 through to P3 (Figures 4I–4L). To further examine *Sema6A* expression, we used mice heterozygous for the *Sema6A* gene trap allele, which can report expression of the trapped gene as *ß-geo* gene expression (Leighton et al., 2001), and found that at least two types of cells expressed *Sema6A* at P1: GABAergic interneurons in L1, as judged by Ctip2 expression (Figure 6D), and in the CP, as judged by the lack of Satb2 expression (Figure 6G), and VZ cells, especially those facing the lateral ventricle (Figure 6H). Neither Cajal-Retzius cells in L1 nor Satb2-positive excitatory cortical neurons expressed Sema6A (Figures 6E–6G).

Owing to the lack of specific antibodies, we could not directly examine the distribution of Sema6A protein responsible for SLN mislocation. However, as an alternative method, we employed a ligand–receptor-binding assay using alkaline phosphatase (AP)-conjugated recombinant protein for the sema domain of PlxnA2 (AP-PlxnA2, Renaud et al., 2008). When AP-PlxnA2 protein was applied to P1 live cortical slices, it bound most strongly to L1 (Figure 6I). Likewise, AP-Sema6A, consisting of the ectodomain of Sema6A and AP (Suto et al., 2005), bound most strongly to L1 (Figure 6I). These results led us to the idea that Sema6A protein is mainly distributed in L1 and functions via binding to PlxnA2/A4 on SLN leading processes extending into L1.

Both GABAergic interneurons and cortical VZ cells can synthesize Sema6A protein in L1. Although the somata of VZ cells are located far from L1, these cells could be a source of Sema6A proteins observed in L1. This idea gains support from the fact that VZ cells transfected with *myc*-tagged *Sema6A* displayed

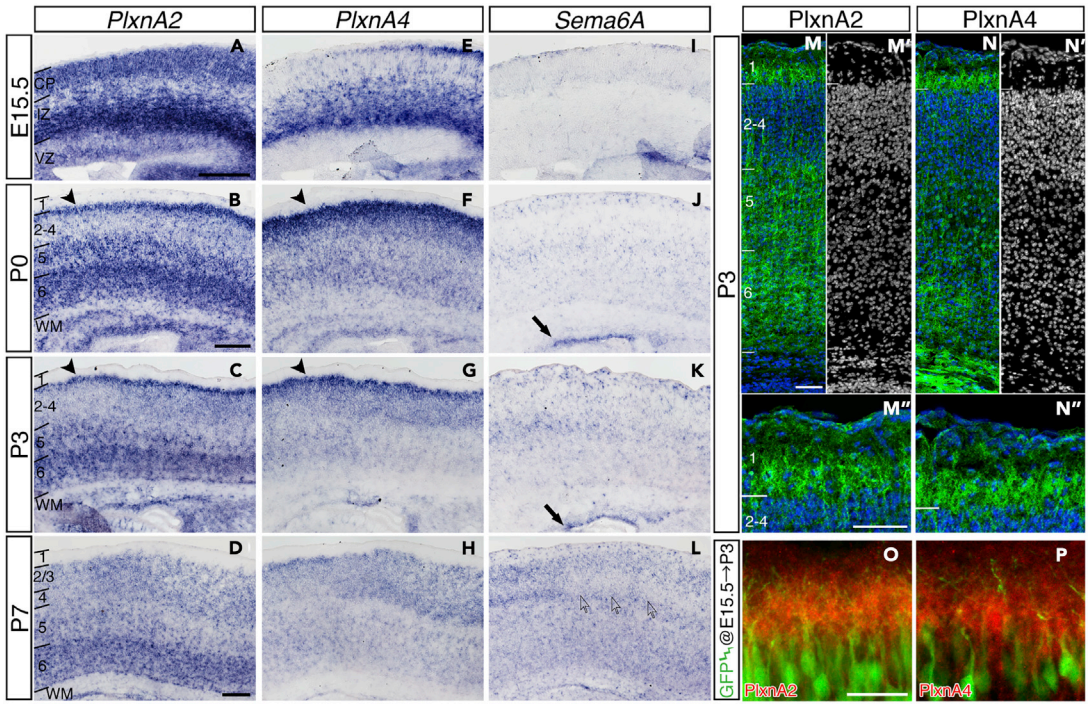

Figure 4. PlxnA2, PlxnA4, and Sema6A Expression at Perinatal Stages

(A–L) *In situ* hybridization analysis of *PlxnA2*, *PlxnA4*, and *Sema6A* mRNA expression at E15.5, P0, P3, and P7 in presumptive S1 area. Both *PlxnA2* and *A4* mRNAs were enriched in the upper part of the CP at P0 and P3 (arrowheads). *PlxnA2* mRNA was also enriched in the deeper part. *Sema6A* mRNA expression was generally scattered throughout the cerebral wall, but was high in the cortical VZ at P0 and P3 (arrows in J and K). Open arrows in (L) point to the location of presumptive barrels in L4. IZ, intermediate zone.

(M–N″) PlxnA2 and PlxnA4 immunoreactivities (green) with nuclear counterstain (blue) at P3 (M and N), nuclear stain alone (M′ and N′), and an enlarged view (M″ and N″). Weak whitish cell nuclear staining in the L5 region in (N) is non-specific, as it was observed after immunostaining without anti-PlxnA2 or anti-A4 antibodies.

(O and P) PlxnA2 and PlxnA4 immunoreactivities (red) with GFP^{+} SNLs (green).

Scale bars: 200 μm in (A, E and I) and (B, C, F, G, J, and K) and (D, H and L), and 50 μm in (M–N′), (M″ and N″) and (O and P).

expression of exogenous Sema6A protein throughout the RG cell processes, including their endfeet, in L1 (Figures S3G–S3K′).

Sema6A Expression in VZ Cells Is Responsible for the Proper Termination of SLN Migration

The above observations indicate that both GABAergic and VZ cells could be sources of Sema6A protein. To identify the Sema6A source responsible for termination of SLN migration, we took a conditional (c) KO approach, using a *Sema6A*-floxed mouse (*Sema6A*$^{fl/fl}$), whose exon 3 is flanked by the *loxP* sequence (Figure S4). As described above, mice lacking exon 3 (*Sema6A*$^{\Delta/\Delta}$) phenocopied the *PlxnA2/A4* dKO mice in terms of SLN mislocation (Figures 7A, 7E, and 7G, n = 3 brains for each genotype, see also Figures 5D, 5H, S2D, and S2E, and S5), indicating that Cre-mediated recombination of this floxed allele indeed disrupted Sema6A functions. We first crossed *Sema6A*$^{\Delta/fl}$ mice with the *Emx1-Cre* line (Iwasato et al., 2008), in which Cre is expressed in VZ cells and excitatory neurons of the pallium, but not in GABAergic interneurons, which are derived from the subpallium (Gorski et al., 2002). The resulting number of Satb2^{+} cells in L1 of *Emx1-Cre*;*Sema6A*$^{\Delta/fl}$ mice was almost identical to that of *Sema6A*$^{\Delta/\Delta}$ mice, indicating that the major cell source of Sema6A regulating SLN positioning is the pallium (Figure 7B, n = 3 brains).

As described above, the *Emx1-Cre* line inactivates *Sema6A* in pallial VZ cells and their descendants in both embryonic and perinatal stages. To remove *Sema6A* specifically in perinatal VZ cells (Figures 4J, 4K, and 6H), we crossed *Sema6A*$^{\Delta/fl}$ mice with the *Nestin-CreER*^{T2} line (Imayoshi et al., 2006), in which *CreER*^{T2}, a tamoxifen-inducible Cre recombinase, is continuously expressed in VZ cells from the embryonic through to the perinatal period. We first confirmed that tamoxifen administration at E17.5 induced

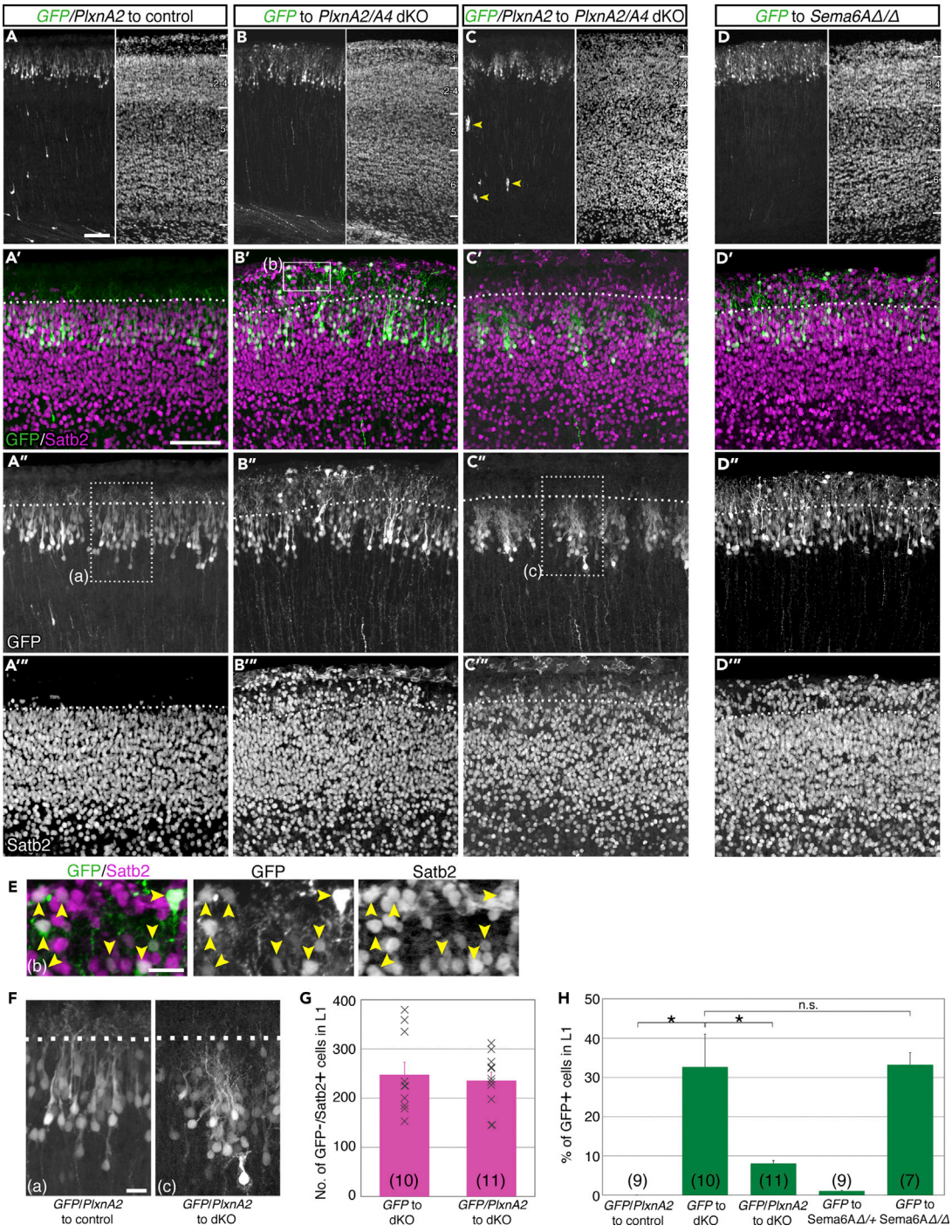

Figure 5. Transfection of SLN Progenitors with *PlxnA2* Rescues SLN Mislocation in *PlxnA2/A4* dKO Mice

(A–C‴) Transfection of SLN progenitors in the VZ with *GFP* alone or a mixture of *GFP* and *PlxnA2* plasmids. IUE was performed on control (A) or dKO mice (B and C) at E15.5 and brains were examined at P3. (A–C) Left and right panels indicate the distribution of GFP$^+$ cells and nuclear counterstain, respectively. (A′–C′) Higher-magnification merged views of GFP fluorescence and Satb2 staining. (A″–C″) GFP and (A‴–C‴) Satb2 views. Dotted lines indicate the L1–L2/3 boundary. The region located within 70 μm from the pial surface was regarded as L1. Note that some PlxnA2/GFP-high$^+$ cells in dKO mice aggregated in the CP (arrowheads in C) and the WM (see Figure S3).

(D) Transfection of *GFP* plasmid into SLN progenitors of *Sema6A*$^{\Delta}$/$^{\Delta}$ mice, by IUE at E15.5; brain was examined at P3. Left and right panels indicate the distribution of GFP$^+$ cells and nuclear counterstain, respectively. (D′) Higher-magnification merged views of GFP fluorescence and Satb2 staining. (D″) GFP and (D‴) Satb2 views.

Figure 5. *Continued*

(E) Higher-magnification views of the region indicated by a rectangle in (B′), indicating that ectopically positioned GFP$^+$ cells were Satb2-positive (arrowheads).

(F) Higher-magnification views of the regions indicated by dotted rectangles in A″ (left panel) and C″ (right panel).

(G) Bar histogram showing the number of GFP$^-$/Satb2$^+$ cells in L1. Cell numbers counted in an individual section are indicated by crosses.

(H) Bar histogram showing the percentage of GFP$^+$ cells in L1 among total GFP$^+$ cells above the WM. In (G and H) three or four sections each from three brains were examined, although two brains were used for *Sema6A*$^{\Delta/\Delta}$. The numbers in parentheses indicate the numbers of sections in each group. Data are represented as mean ± SEM. *$p < 0.05$ (one-way ANOVA followed by Tukey's post-hoc test). n.s., not significant. The results of statistical analyses are indicated only on the focused groups.

Scale bars: 100 μm in (A–D) and (A′–D‴), and 20 μm in (E) and (F).

recombination almost exclusively in VZ cells (Figures S6A–S6D). We then administered tamoxifen to *Nestin-CreER*^{T2}; *Sema6A*$^{\Delta/fl}$ mice at E17.5 and found that *Sema6A* was indeed inactivated in VZ cells (Figures S6E and S6F). In these mice, the SLN mislocation phenotype observed in *Sema6A*$^{\Delta/\Delta}$ was recapitulated (Figures 7D and 7G, $n = 3$ brains). As a control, SLN-targeted *Sema6A* inactivation was carried out by IUE with *pDCX-Cre* plasmid, which drives Cre expression in postmitotic premigratory neurons (Franco et al., 2011). As expected, this did not affect SLN positioning (Figure S6G, $n = 3$ brains). Taken together, our findings indicate that the source of Sema6A responsible for termination of SLN migration is cortical VZ cells.

Reelin$^+$ Cajal-Retzius Cells and Reelin Signaling Pathway Are Unchanged

Reelin is essential for proper laminar positioning of cortical neurons (D'Arcangelo et al., 1995). Several reelin-related mutant mice exhibit a mis1location phenotype of SLNs resembling *Sema6A* KO (*Sema6A*$^{-/-}$ and *Sema6A*$^{\Delta/\Delta}$) *and PlxnA2/A4* dKO mice (Ha et al., 2017; Hack et al., 2007; Herrick and Cooper, 2002; Hirota et al., 2018; Kohno et al., 2015). This raises the possibility that reelin signaling is altered in *Sema6A* KO and *PlxnA2/A4* dKO mice. We found that Cajal-Retzius cells, a major source of reelin in L1 of developing mouse (Ogawa et al., 1995), were distributed normally in *PlxnA2/A4* dKO mice (Figures S7A–S7D″). There was no difference in their number between control (11.3 ± 0.9, in a 400-μm-wide MZ at P1, $n = 6$ strips, 2 brains) and *PlxnA2/A4* dKO mice (10.8 ± 1.0, $n = 6$ strips, 2 brains). Furthermore, there were no notable changes in reelin-dependent cells or reelin signaling in these mice: (1) the morphology of RG cell processes, which is affected by reelin signaling (Chai et al., 2015; Hartfuss et al., 2003), appeared normal (Figures S7E and S7F) in *PlxnA2/A4* dKO mice and (2) the expression profiles of Dab1, which is an essential component of the canonical reelin signaling pathway and whose expression level is regulated by reelin signaling (Arnaud et al., 2003; Howell et al., 1999, 2000), were unaffected both in *Sema6A*$^{-/-}$ and in *PlxnA2/A4* dKO mice (Figures S7G–S7K). These findings argue against the possibility that mislocation of SLNs is mediated by attenuation of reelin signaling.

DISCUSSION

In this study, we have shown that many SLNs were mislocated in L1 of *PlxnA2/A4* dKO and *Sema6A* KO/cKO mice. This is most likely to be a result of overmigration past their final destinations. Given that PlxnA2/A4 and Sema6A were expressed in migrating cortical neurons and RG cells, respectively, the most likely explanation for the phenotype is that the normal detachment of migrating SLNs from RG endfeet was abrogated in these mice due to a lack of repulsive interactions caused by Sema6A–PlxnA2/A4 signaling (Figure 7H). We hypothesize that this detachment is critical for SLNs for their migration termination at their final destinations.

Functional Requirement for PlxnA2/A4 in Migrating SLNs and for Sema6A in the RG Scaffold

Sema6A can interact with PlxnA2/A4 in either *cis* (on the same cell) or *trans* (on different cells) to transduce their signals (Battistini and Tamagnone, 2016). These two types of interactions seem to differently regulate the strength or functionality of the signals (Battistini and Tamagnone, 2016; Haklai-Topper et al., 2010; Suto et al., 2007). Typically, Sema6A–PlxnA2/A4 *trans*-interaction transduces predominantly repulsive signaling (Battistini and Tamagnone, 2016). In this context, it is important to know whether or not Sema6A and PlxnA2/A4 are expressed on the same cells. We found that PlxnA2, and probably A4 as well, act cell autonomously in SLNs. On the other hand, these cells do not express Sema6A. Moreover, SLN-specific inactivation of Sema6A caused no notable phenotype, supporting a non-cell-autonomous function of Sema6A. Thus, Sema6A most likely functions in *trans* with PlxnA2/A4 of the SLNs, which probably elicits repulsive signaling.

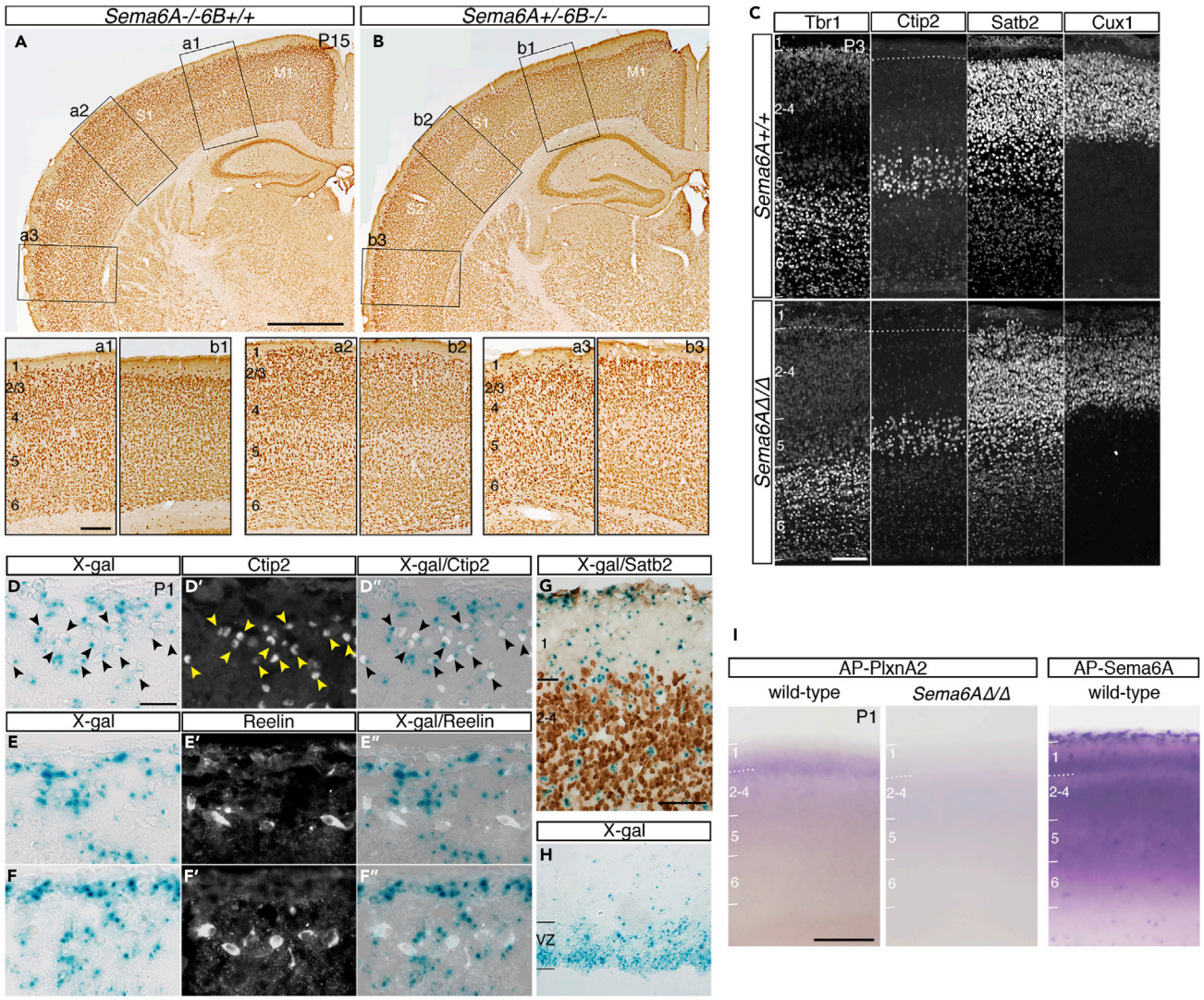

Figure 6. Cortical Cytoarchitecture of *Sema6A* Mutant Mice, Identity of Sema6A-Expressing Cells, and Sema6A Protein Localization

(A and B) NeuN staining of a coronal section from a P15 mouse homozygous for *Sema6A* gene trap allele (A) and a compound mutant mouse heterozygous for *Sema6A* gene trap allele and homozygous for *Sema6B* knockout allele (B). The lower panels of (A and B) show higher-magnification views of the dorsal (a1 and b1), dorsolateral (a2 and b2), and lateral (a3 and b3) regions indicated by rectangles in (A and B).

(C) Immunostaining of coronal sections from P3 wild-type and *Sema6A*$^{\Delta/\Delta}$ mice using cortical layer markers. Tbr1 is a marker for L6 neurons. For Ctip2, Satb2, and Cux1, see legend of Figure 2. Dotted lines indicate the L1–L2/3 boundary. Compare with Figure S2B, and see also Figures S4 and S5.

(D–H) Sema6A-expressing cells in the cerebral cortex at P1. These were identified by X-gal staining (blue) in sections taken from heterozygotes of *Sema6A* gene trap mice. As the trapped gene is fused to β-geo (a fusion between β-galactosidase and neomycin phosphotransferase, Leighton et al., 2001), cells expressing endogenous Sema6A can be identified by β-geo activity, which is retained within the endoplasmic reticulum. (D–F″) X-gal staining in L1 (D–F), anti-Ctip2 (D′) or anti-reelin antibody staining (E′ and F′), and merged views (D″–F″). Note that because Ctip2 expression marks a subset of GABAergic interneurons and L5 excitatory neurons (Arlotta et al., 2005), it is likely that Ctip2^{+} cells in L1 (yellow arrowheads) are GABAergic cells. (G) X-gal staining with an anti-Satb2 antibody staining (brown). (H) X-gal staining in the VZ.

(I) Binding profiles of AP-PlxnA2 on wild-type and *Sema6A*$^{\Delta/\Delta}$ cortical slices, and of AP-Sema6A on a wild-type cortical slice, at P1. No specific binding of AP-PlxnA2 was observed on Sema6A$^{\Delta/\Delta}$ slices, verifying a Sema6A–PlxnA2 molecular interaction.

Scale bars: 1 mm in (A and B), 200 μm in (a1–b3), 100 μm in (C) and (I), 25 μm in (D–F″), and 50 μm in (G and H).

Several lines of evidence indicate that the major source of Sema6A is cortical VZ cells. This is because conditional removal of *Sema6A* from cells of pallial origin using *Emx1-Cre* driver mice caused a mislocation phenotype resembling that in *Sema6A* KO mice. Moreover, selective removal of *Sema6A* from VZ cells at a late embryonic stage induced neuronal invasion into L1 (Figure 7). Although a minor contribution of

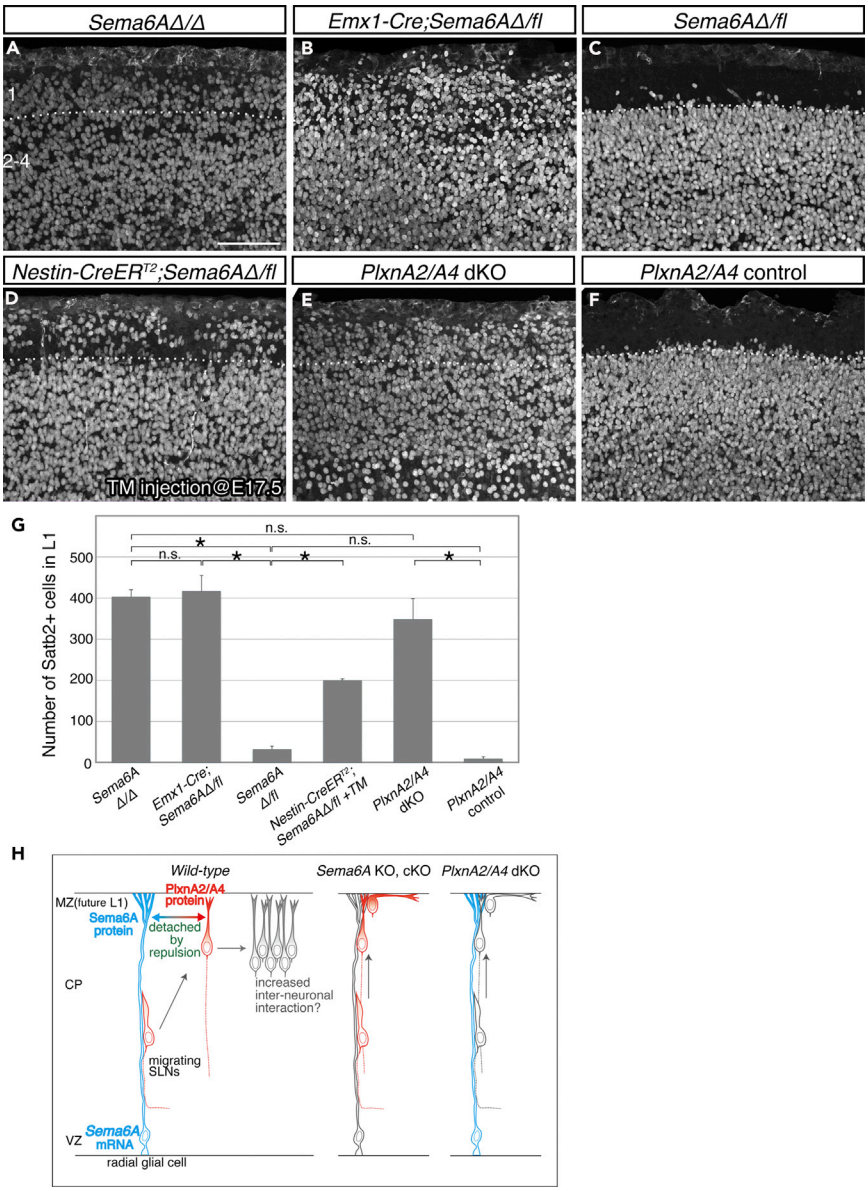

Figure 7. *Sema6A* Mice Reveal a Requirement for *Sema6A* in VZ Cells for Proper Termination of SLN Migration

(A–F) Satb2 staining of the presumptive S1 area of (A) *Sema6A*$^{\Delta/\Delta}$, (B) *Emx1-Cre*; *Sema6A*$^{\Delta/fl}$, (C) *Sema6A*$^{\Delta/fl}$, (D) *Nestin-CreER*^{T2}; *Sema6A*$^{\Delta/fl}$ (administered tamoxifen at E17.5), (E) *PlxnA2*$^{-/-}$*A4*$^{-/-}$, and (F) *PlxnA2*$^{+/-}$*A4*$^{+/-}$ mice at P3. Dotted lines indicate the L1–L2/3 boundary. Note that SLNs of *Sema6A*$^{\Delta/\Delta}$, *Emx1-Cre*; *Sema6A*$^{\Delta/fl}$, *Nestin-CreER*^{T2}; *Sema6A*$^{\Delta/fl}$, and *PlxnA2*$^{-/-}$*A4*$^{-/-}$ dKO mice were less tightly packed than those of the control groups.

(G) Bar histogram showing the number of Satb2^{+} cells in L1 in a 450-μm-wide strip. Three sections each from three brains were examined. Data are represented as mean ± SEM. *$p < 0.05$ (one-way ANOVA followed by Tukey's post-hoc test). n.s., not significant. In *Nestin-CreER*^{T2}; *Sema6A*$^{\Delta/fl}$ cKO mice, the phenotype was milder than that in *Sema6A* KO mice. This may be due to insufficient recombination, because tamoxifen-induced Cre recombination is not very effective in general (Vooijs et al., 2001). See also Figure S6. Scale bar, 100 μm in (A–F).

(H) Model for mislocation of SLNs in *Sema6A* KO/cKO and *PlxnA2/A4* dKO mice. The illustration indicates the proposed mechanism for termination of neuronal migration and proper positioning of SLNs through Sema6A (blue)–PlxnA2/A4 (red) interaction. (Left) SLNs migrate toward the pial surface along fibers of RG cells, whose cell bodies are located in the VZ. Sema6A protein synthesized in VZ cells travel distally along the fibers at the stage when SLNs reach the top of the CP. Meanwhile, PlxnA2/A4 expression in SLNs is up-regulated and concentrated on apical processes extending into L1.

Figure 7. *Continued*

(Middle and right) In both *Sema6A* KO/cKO and *PlxnA2/A4* dKO mice, SLNs appear to migrate beyond their final destination, thus invading L1. We propose that L1 Sema6A on RG cell fibers acts with PlxnA2/A4 on leading processes of SLNs to detach them from the fibers, which is a key step for proper termination of migration.

Sema6A from other cells, such as GABAergic cells and immature glial cells, cannot be ruled out, our results collectively support the conclusion that cortical VZ cells are the major source of Sema6A required for termination of SLN migration.

The next question that arises is where the Sema6A–PlexinA2/A4 interaction occurs. Given that cortical VZ cells extend RG fibers reaching the pial surface during the embryonic and early postnatal periods, and that *Sema6A* mRNA expression in VZ cells was high at the time when SLNs reach their target, it is likely that this interaction occurs at L1 and nearby. Indeed, AP-PlxnA2 preferentially bound to the region of L1 and nearby where binding of AP-Sema6A also occurred.

Independence of SLN Mislocation from Thalamocortical Projection Error

Abnormal thalamocortical projection to L1, which can be observed at P2, has been reported in *Sema6A*$^{-/-}$ and *PlxnA2/A4* dKO mice (Little et al., 2009; Mitsogiannis et al., 2017; Rünker et al., 2011), raising the possibility that the phenotypes observed here occurred as a consequence this projection error. However, we observed almost no such aberrant thalamocortical projection in *Sema6A* cKO mice crossed with *Emx1-Cre* mice (data not shown).

Critical Role of Sema6A–PlxnA2/A4 Interaction in Termination of Neuronal Migration

How does Sema6A–PlxnA2/A4 interaction contribute to establishing correct positioning of SLNs? We consider that the mislocation of SLNs observed in KO mice is a consequence of a failure in termination of migration. Goffinet (1984) proposed that when neurons terminate migration, the affinity between the neurons and the RG fibers is attenuated, thus leading to detachment of migrating neurons from their glial substrate. The present study is consistent with this hypothesis: first, PlxnA2/A4 expression in SLNs appeared to be up-regulated at the terminal phase of migration, whereas Sema6A was concurrently supplied from VZ cells to their endfeet, and second, both Sema6A and PlxnA2/4 appeared to be localized to the site where the detachment probably takes place. Given that Sema6A–PlxnA2/A4 *trans*-interactions generally mediate a repulsive response (Battistini and Tamagnone, 2016), the most likely scenario is that SLNs terminate migration as a result of Sema6A–PlxnA2/A4 interactions, which may reduce the affinity between migrating SLNs and their RG substrates.

Arguably, the fact that PlxnA2/A4 mRNAs are broadly expressed in the upper layers from P0 raises the possibility that SLN mislocation occurred as a secondary effect. We cannot completely exclude this possibility. However, highly localized distribution of Sema6A in the L1 region indicates that Sema6A can directly interact with PlxnA2/A4 expressed by SLNs. Further studies are needed to validate this view.

An additional prediction by Goffinet (1984) is that an enhancement of neuron–neuron adhesion would contribute to neuronal detachment from the substrate. Our findings are consistent with this idea: SLNs were less densely packed in both *Sema6A*$^{\Delta/\Delta}$ and *PlxnA2/A4* dKO mice at P3 (e.g., Figure 7), whereas forced PlxnA2 expression in SLNs of the dKO mice induced aggregation of these neurons (e.g., GFP/PlxnA2-high cells, Figure S3F). This apparent up-regulation of neuronal adhesion may be a direct consequence of Sema6A–PlxnA2/A4 signaling, because Plxn signaling also mediates axon fasciculation (Rünker et al., 2008, 2011; Suto et al., 2005), probably by enhancing axon-axon adhesiveness via homophilic binding (Ohta et al., 1995). Alternatively, the neuronal aggregation may have been a secondary result of a reduction of neuron–glia adhesion. In any case, the relative strength of adhesiveness among different cell types is integral to understanding the termination of migration and the consequent correct positioning of SLNs.

Possible Downstream Signaling Pathway of Sema6A–PlxnA2/A4

Plexin family members are known to work via small GTPases, which elicit repulsive effects on axons by regulating cytoskeletal and adhesive dynamics (Alto and Terman, 2017). In addition, in *Drosophila*, Mical, an oxidoreductase enzyme that disassembles F-actin, has been shown to directly interact with the cytoplasmic region of PlxnA and mediate a repulsive activity (Yang and Terman, 2013). Interestingly, in mice and chickens, Sema-mediated repellent interactions between boundary cap cells and immature spinal motor

neurons act as a stop signal to regulate positioning of motor neurons (Bron et al., 2007; Mauti et al., 2007). This repulsive signal is mediated by MICAL3 (Bron et al., 2007). It would be interesting to examine whether the same effector also functions in Sema6A–PlxnA2/A4 signaling for proper SLN positioning.

Independence of Sema6A–PlxnA2/A4 Signaling from Reelin Signaling

In the present study, we found no obvious interactions between Sema6A–PlxnA2/A4 and reelin signaling. Although cortical phenotypes of mice in which either signaling pathway is mutated are somewhat similar, we noticed on closer examination that their phenotypes are distinguishable. For example, in $Reln^{\Delta C\text{-}KI}$ mice (Kohno et al., 2015), SLNs rarely reach beneath the pial surface, whereas they do so in *Sema6A* KO/cKO and *PlxnA2/A4* dKO mice. It is conceivable that these two individual signaling pathways regulate termination of neuronal migration independently or additively to ensure proper development of the laminar architecture of the cortex.

Implied Existence of a Specific Mechanism for Termination of SLN Migration

Sema6A–PlxnA2/A4 signaling is required for superficial but not deeper layer neurons. We consider two alternative scenarios for this differential effect: (1) neurons in different layers use different signaling pathways for detachment from RG fibers and (2) termination of SLN migration requires a specific mechanism in addition to the termination mechanisms required for neurons in other layers. For example, the last-born SLNs are special in terms of lacking a following migratory neuron. Further studies are needed to uncover whether a temporally regulated change in the interaction between neurons and their substrate is a general mechanism for termination of neuronal migration in the cortex.

Limitations of the Study

We found evidence that an interaction between Sema6A and PlxnA2/A4, which are expressed on RG cells and SLNs, respectively, regulates laminar positioning of SLNs. We speculate that migrating SLNs become detached from their substrate, RG, on arrival at their final positions, due to the repulsive interaction between Sema6A and PlxnA2/A4. However, technical difficulty prevented us from confirming this by directly observing the process of detachment itself. Analysis of downstream effector(s) of Sema6A–PlxnA2/A4 signaling may also be needed for clarifying the process in mechanistic terms in the future.

METHODS

All methods can be found in the accompanying Transparent Methods supplemental file.

SUPPLEMENTAL INFORMATION

Supplemental Information can be found online at https://doi.org/10.1016/j.isci.2019.10.034.

ACKNOWLEDGMENTS

We thank Drs. Hajime Fujisawa for his initial suggestion on the phenotype of *PlxnA2/A4* mutant mice and Sadao Shiosaka for his generous support in the initial stage of this study. We also thank Drs. Fujio Murakami and Yan Zhu for critical reading of the manuscript; Tomohiro Namikawa for his initial help in mouse analysis; Fumikazu Suto for $PlxnA2^{-/-}$ and $PlxnA4^{-/-}$ mice, cDNAs of *PlxnA2*, *PlxnA4*, and *Sema6A*, and antibodies for PlxnA2 and PlxnA4; Kevin J. Mitchell for $Sema6A^{-/-}$; Yutaka Yoshida for $Sema6B^{-/-}$; Takuji Iwasato for *Emx1-Cre* and Ryoichiro Kageyama for $Nestin\text{-}CreER^{T2}$ mice; Masaharu Ogawa for anti-reelin and Yasuyoshi Arimatsu for anti-nestin antibodies; Alain Chédotal for *AP-PlxnA2* and AP-*Sema6A* plasmids; and Ms. Nobuko Hattori for technical assistance. Some of the confocal images were acquired at the Spectrography and Bioimaging Facility, NIBB Core Research Facilities. This work was supported by a Grant-in-Aid from JSPS_KAKENHI (25430020) and the NIG-JOINT Collaboration Research Grants (2013-A, 2017-A) to Y.H., JSPS_KAKENHI (17H06311) to Y.K. and (16H04659, 17H05587, 17H05776) to T.H., and the Takeda Science Foundation to A.S.

AUTHOR CONTRIBUTIONS

Conceptualization, Methodology, and Investigation, Y.H. and T. Kawasaki; Resources, T.A., G.S., T. Kohno, M.H., and A.S.; Writing – Original Draft, Y.H.; Writing – Review & Editing, Y.H., T. Kawasaki, and T.H. with feedback from all authors; Funding Acquisition, Y.H., A.S., Y.K., and T.H.; Supervision, Y.K. and T.H.

DECLARATION OF INTERESTS

The authors declare no competing interests.

Received: November 12, 2018
Revised: August 30, 2019
Accepted: October 16, 2019
Published: November 22, 2019

REFERENCES

Alto, L.T., and Terman, J.R. (2017). Semaphorins and their signaling mechanisms. Methods Mol. Biol. *1493*, 1–25.

Arlotta, P., Molyneaux, B.J., Chen, J., Inoue, J., Kominami, R., and Macklis, J.D. (2005). Neuronal subtype-specific genes that control corticospinal motor neuron development in vivo. Neuron *45*, 207–221.

Arnaud, L., Ballif, B.A., and Cooper, J.A. (2003). Regulation of protein tyrosine kinase signaling by substrate degradation during brain development. Mol. Cell. Biol. *23*, 9293–9302.

Barkovich, A.J., Dobyns, W.B., and Guerrini, R. (2015). Malformations of cortical development and epilepsy. Cold Spring Harb. Perspect. Med. *5*, a022392.

Barkovich, A.J., Guerrini, R., Kuzniecky, R.I., Jackson, G.D., and Dobyns, W.B. (2012). A developmental and genetic classification for malformations of cortical development: update 2012. Brain *135*, 1348–1369.

Battistini, C., and Tamagnone, L. (2016). Transmembrane semaphorins, forward and reverse signaling: have a look both ways. Cell Mol. Life Sci. *73*, 1609–1622.

Belle, M., Parray, A., Belle, M., Chedotal, A., and Nguyen-Ba-Charvet, K.T. (2016). PlexinA2 and Sema6A are required for retinal progenitor cell migration. Dev. Growth Differ. *58*, 492–502.

Britanova, O., de Juan Romero, C., Cheung, A., Kwan, K.Y., Schwark, M., Gyorgy, A., Vogel, T., Akopov, S., Mitkovski, M., Agoston, D., et al. (2008). Satb2 is a postmitotic determinant for upper-layer neuron specification in the neocortex. Neuron *57*, 378–392.

Bron, R., Vermeren, M., Kokot, N., Andrews, W., Little, G.E., Mitchell, K.J., and Cohen, J. (2007). Boundary cap cells constrain spinal motor neuron somal migration at motor exit points by a semaphoring-plexin mechanism. Neural Dev. *2*, 21.

Chai, X., Fan, L., Shao, H., Lu, X., Zhang, W., Li, J., Wang, J., Chen, S., Frotscher, M., and Zhao, S. (2015). Reelin induces branching of neurons and radial glial cells during corticogenesis. Cereb. Cortex *25*, 3640–3653.

Costa, C., Harding, B., and Copp, A.J. (2001). Neuronal migration defects in the Dreher (Lmx1a) mutant mouse: role of disorders of the glial limiting membrane. Cereb. Cortex *11*, 498–505.

D'Arcangelo, G. (2005). The reeler mouse: anatomy of a mutant. Int. Rev. Neurobiol. *71*, 383–417.

D'Arcangelo, G., Miao, G.G., Chen, S.C., Soares, H.D., Morgan, J.I., and Curran, T. (1995). A protein related to extracellular matrix proteins deleted in the mouse mutant reeler. Nature *374*, 719–723.

Evsyukova, I., Plestant, C., and Anton, E.S. (2013). Integrative mechanisms of oriented neuronal migration in the developing brain. Annu. Rev. Cell Dev. Biol. *29*, 299–353.

Faulkner, R.L., Low, L.K., Liu, X.B., Coble, J., Jones, E.G., and Cheng, H.J. (2008). Dorsal turning of motor corticospinal axons at the pyramidal decussation requires plexin signaling. Neural Dev. *3*, 21.

Franco, S.J., Martinez-Garay, I., Gil-Sanz, C., Harkins-Perry, S.R., and Muller, U. (2011). Reelin regulates cadherin function via Dab1/Rap1 to control neuronal migration and lamination in the neocortex. Neuron *69*, 482–497.

Goffinet, A.M. (1984). Events governing organization of postmigratory neurons: studies on brain development in normal and reeler mice. Brain Res. *319*, 261–296.

Gongidi, V., Ring, C., Moody, M., Brekken, R., Sage, E.H., Rakic, P., and Anton, E.S. (2004). SPARC-like 1 regulates the terminal phase of radial glia-guided migration in the cerebral cortex. Neuron *41*, 57–69.

Goodman, C.S., Kolodkin, A.L., Luo, Y., Püschel, A.W., and Raper, J.A. (1999). Unified nomenclature for the semaphorins/collapsins. Cell *97*, 551–552.

Gorski, J.A., Talley, T., Qiu, M., Puelles, L., Rubenstein, J.L., and Jones, K.R. (2002). Cortical excitatory neurons and glia, but not GABAergic neurons, are produced in the Emx1-expressing lineage. J. Neurosci. *22*, 6309–6314.

Ha, S., Tripathi, P.P., Mihalas, A.B., Hevner, R.F., and Beier, D.R. (2017). C-terminal region truncation of RELN disrupts an interaction with VLDLR, causing abnormal development of the cerebral cortex and Hippocampus. J. Neurosci. *37*, 960–971.

Hack, I., Hellwig, S., Junghans, D., Brunne, B., Bock, H.H., Zhao, S., and Frotscher, M. (2007). Divergent roles of ApoER2 and Vldlr in the migration of cortical neurons. Development *134*, 3883–3891.

Haklai-Topper, L., Mlechkovich, G., Savariego, D., Gokhman, I., and Yaron, A. (2010). Cis interaction between Semaphorin6A and Plexin-A4 modulates the repulsive response to Sema6A. EMBO J. *29*, 2635–2645.

Hartfuss, E., Forster, E., Bock, H.H., Hack, M.A., Leprince, P., Luque, J.M., Herz, J., Frotscher, M., and Gotz, M. (2003). Reelin signaling directly affects radial glia morphology and biochemical maturation. Development *130*, 4597–4609.

Hatanaka, Y., Hisanaga, S., Heizmann, C.W., and Murakami, F. (2004). Distinct migratory behavior of early- and late-born neurons derived from the cortical ventricular zone. J. Comp. Neurol. *479*, 1–14.

Herms, J., Anliker, B., Heber, S., Ring, S., Fuhrmann, M., Kretzschmar, H., Sisodia, S., and Muller, U. (2004). Cortical dysplasia resembling human type 2 lissencephaly in mice lacking all three APP family members. EMBO J. *23*, 4106–4115.

Herrick, T.M., and Cooper, J.A. (2002). A hypomorphic allele of dab1 reveals regional differences in reelin-Dab1 signaling during brain development. Development *129*, 787–796.

Hirota, Y., Kubo, K., Fujino, T., Yamamoto, T.T., and Nakajima, K. (2018). ApoER2 controls not only neuronal migration in the intermediate zone but also termination of migration in the developing cerebral cortex. Cereb. Cortex *28*, 223–235.

Howell, B.W., Herrick, T.M., and Cooper, J.A. (1999). Reelin-induced tyrosine phosphorylation of disabled 1 during neuronal positioning. Genes Dev. *13*, 643–648.

Howell, B.W., Herrick, T.M., Hildebrand, J.D., Zhang, Y., and Cooper, J.A. (2000). Dab1 tyrosine phosphorylation sites relay positional signals during mouse brain development. Curr. Biol. *10*, 877–885.

Huang, Y., Song, N.N., Lan, W., Hu, L., Su, C.J., Ding, Y.Q., and Zhang, L. (2013). Expression of transcription factor Satb2 in adult mouse brain. Anat. Rec. (Hoboken) *296*, 452–461.

Imayoshi, I., Ohtsuka, T., Metzger, D., Chambon, P., and Kageyama, R. (2006). Temporal regulation of Cre recombinase activity in neural stem cells. Genesis *44*, 233–238.

Iwasato, T., Inan, M., Kanki, H., Erzurumlu, R.S., Itohara, S., and Crair, M.C. (2008). Cortical adenylyl cyclase 1 is required for thalamocortical synapse maturation and aspects of layer IV barrel development. J. Neurosci. *28*, 5931–5943.

Jeong, S.J., Luo, R., Singer, K., Giera, S., Kreidberg, J., Kiyozumi, D., Shimono, C., Sekiguchi, K., and Piao, X. (2013). GPR56 functions together with alpha3beta1 integrin in regulating cerebral cortical development. PLoS One *8*, e68781.

Kerjan, G., Dolan, J., Haumaitre, C., Schneider-Maunoury, S., Fujisawa, H., Mitchell, K.J., and

Chedotal, A. (2005). The transmembrane semaphorin Sema6A controls cerebellar granule cell migration. Nat. Neurosci. *8*, 1516–1524.

Kohno, T., Honda, T., Kubo, K., Nakano, Y., Tsuchiya, A., Murakami, T., Banno, H., Nakajima, K., and Hattori, M. (2015). Importance of Reelin C-terminal region in the development and maintenance of the postnatal cerebral cortex and its regulation by specific proteolysis. J. Neurosci. *35*, 4776–4787.

Leighton, P.A., Mitchell, K.J., Goodrich, L.V., Lu, X., Pinson, K., Scherz, P., Skarnes, W.C., and Tessier-Lavigne, M. (2001). Defining brain wiring patterns and mechanisms through gene trapping in mice. Nature *410*, 174–179.

Little, G.E., Lopez-Bendito, G., Runker, A.E., Garcia, N., Pinon, M.C., Chedotal, A., Molnar, Z., and Mitchell, K.J. (2009). Specificity and plasticity of thalamocortical connections in Sema6A mutant mice. PLoS Biol. *7*, e98.

Luuk, H., Koks, S., Plaas, M., Hannibal, J., Rehfeld, J.F., and Vasar, E. (2008). Distribution of Wfs1 protein in the central nervous system of the mouse and its relation to clinical symptoms of the wolfram syndrome. J. Comp. Neurol. *509*, 642–660.

Matsuoka, R.L., Nguyen-Ba-Charvet, K.T., Parray, A., Badea, T.C., Chedotal, A., and Kolodkin, A.L. (2011). Transmembrane semaphorin signalling controls laminar stratification in the mammalian retina. Nature *470*, 259–263.

Mauti, O., Domaniskaya, E., Andermatt, I., Sadhu, R., and Stoeckli, E.T. (2007). Semaphorin6A acts as a gate keeper between the central and the peripheral nervous system. Neural Dev. *2*, 28.

Mitsogiannis, M.D., Little, G.E., and Mitchell, K.J. (2017). Semaphorin-Plexin signaling influences early ventral telencephalic development and thalamocortical axon guidance. Neural Dev. *12*, 6.

Moers, A., Nurnberg, A., Goebbels, S., Wettschureck, N., and Offermanns, S. (2008). Galpha12/Galpha13 deficiency causes localized overmigration of neurons in the developing cerebral and cerebellar cortices. Mol. Cell. Biol. *28*, 1480–1488.

Moffat, J.J., Ka, M., Jung, E.M., and Kim, W.Y. (2015). Genes and brain malformations associated with abnormal neuron positioning. Mol. Brain *8*, 72.

Murakami, Y., Suto, F., Shimizu, M., Shinoda, T., Kameyama, T., and Fujisawa, H. (2001). Differential expression of plexin-A subfamily members in the mouse nervous system. Dev. Dyn. *220*, 246–258.

Nakagawa, N., Yagi, H., Kato, K., Takematsu, H., and Oka, S. (2015). Ectopic clustering of Cajal-Retzius and subplate cells is an initial pathological feature in Pomgnt2-knockout mice, a model of dystroglycanopathy. Sci. Rep. *5*, 11163.

Nieto, M., Monuki, E.S., Tang, H., Imitola, J., Haubst, N., Khoury, S.J., Cunningham, J., Gotz, M., and Walsh, C.A. (2004). Expression of Cux-1 and Cux-2 in the subventricular zone and upper layers II-IV of the cerebral cortex. J. Comp. Neurol. *479*, 168–180.

Niewmierzycka, A., Mills, J., St-Arnaud, R., Dedhar, S., and Reichardt, L.F. (2005). Integrin-linked kinase deletion from mouse cortex results in cortical lamination defects resembling cobblestone lissencephaly. J. Neurosci. *25*, 7022–7031.

Niwa, H., Yamamura, K., and Miyazaki, J. (1991). Efficient selection for high-expression transfectants with a novel eukaryotic vector. Gene *108*, 193–199.

Ogawa, M., Miyata, T., Nakajima, K., Yagyu, K., Seike, M., Ikenaka, K., Yamamoto, H., and Mikoshiba, K. (1995). The reeler gene-associated antigen on Cajal-Retzius neurons is a crucial molecule for laminar organization of cortical neurons. Neuron *14*, 899–912.

Ohta, K., Mizutani, A., Kawakami, A., Murakami, Y., Kasuya, Y., Takagi, S., Tanaka, H., and Fujisawa, H. (1995). Plexin: a novel neuronal cell surface molecule that mediates cell adhesion via a homophilic binding mechanism in the presence of calcium ions. Neuron *14*, 1189–1199.

Ohtaka-Maruyama, C., and Okado, H. (2015). Molecular pathways underlying projection neuron production and migration during cerebral cortical development. Front. Neurosci. *9*, 447.

Renaud, J., Kerjan, G., Sumita, I., Zagar, Y., Georget, V., Kim, D., Fouquet, C., Suda, K., Sanbo, M., Suto, F., et al. (2008). Plexin-A2 and its ligand, Sema6A, control nucleus-centrosome coupling in migrating granule cells. Nat. Neurosci. *11*, 440–449.

Rünker, A.E., Little, G.E., Suto, F., Fujisawa, H., and Mitchell, K.J. (2008). Semaphorin-6A controls guidance of corticospinal tract axons at multiple choice points. Neural Dev. *3*, 34.

Rünker, A.E., O'Tuathaigh, C., Dunleavy, M., Morris, D.W., Little, G.E., Corvin, A.P., Gill, M., Henshall, D.C., Waddington, J.L., and Mitchell, K.J. (2011). Mutation of Semaphorin-6A disrupts limbic and cortical connectivity and models neurodevelopmental psychopathology. PLoS One *6*, e26488.

Sekine, K., Kubo, K., and Nakajima, K. (2014). How does Reelin control neuronal migration and layer formation in the developing mammalian neocortex? Neurosci. Res. *86*, 50–58.

Sekine, K., Tabata, H., and Nakajima, K. (2013). Cell polarity and initiation of migration. In Comprehensive Developmental Neuroscience: Cellular Migration and Formation of Neuronal Connections, J.L. Rubenstein and P. Rakic, eds. (Academic Press), pp. 231–244.

Smart, I.H., and Smart, M. (1982). Growth patterns in the lateral wall of the mouse telencephalon: I. Autoradiographic studies of the histogenesis of the isocortex and adjacent areas. J. Anat. *134*, 273–298.

Suto, F., Ito, K., Uemura, M., Shimizu, M., Shinkawa, Y., Sanbo, M., Shinoda, T., Tsuboi, M., Takashima, S., Yagi, T., et al. (2005). Plexin-a4 mediates axon-repulsive activities of both secreted and transmembrane semaphorins and plays roles in nerve fiber guidance. J. Neurosci. *25*, 3628–3637.

Suto, F., Murakami, Y., Nakamura, F., Goshima, Y., and Fujisawa, H. (2003). Identification and characterization of a novel mouse plexin, plexin-A4. Mech. Dev. *120*, 385–396.

Suto, F., Tsuboi, M., Kamiya, H., Mizuno, H., Kiyama, Y., Komai, S., Shimizu, M., Sanbo, M., Yagi, T., Hiromi, Y., et al. (2007). Interactions between plexin-A2, plexin-A4, and semaphorin 6A control lamina-restricted projection of hippocampal mossy fibers. Neuron *53*, 535–547.

Tawarayama, H., Yoshida, Y., Suto, F., Mitchell, K.J., and Fujisawa, H. (2010). Roles of semaphorin-6B and plexin-A2 in lamina-restricted projection of hippocampal mossy fibers. J. Neurosci. *30*, 7049–7060.

Toyofuku, T., Yoshida, J., Sugimoto, T., Yamamoto, M., Makino, N., Takamatsu, H., Takegahara, N., Suto, F., Hori, M., Fujisawa, H., et al. (2008). Repulsive and attractive semaphorins cooperate to direct the navigation of cardiac neural crest cells. Dev. Biol. *321*, 251–262.

Vooijs, M., Jonkers, J., and Berns, A. (2001). A highly efficient ligand-regulated Cre recombinase mouse line shows that LoxP recombination is position dependent. EMBO Rep. *2*, 292–297.

Yang, T., and Terman, J.R. (2013). Regulating small G protein signaling to coordinate axon adhesion and repulsion. Small GTPases *4*, 34–41.

ISCI, Volume *21*

Supplemental Information

Semaphorin 6A–Plexin A2/A4 Interactions with Radial Glia Regulate Migration Termination of Superficial Layer Cortical Neurons

Yumiko Hatanaka, Takahiko Kawasaki, Takaya Abe, Go Shioi, Takao Kohno, Mitsuharu Hattori, Akira Sakakibara, Yasuo Kawaguchi, and Tatsumi Hirata

Figure S1

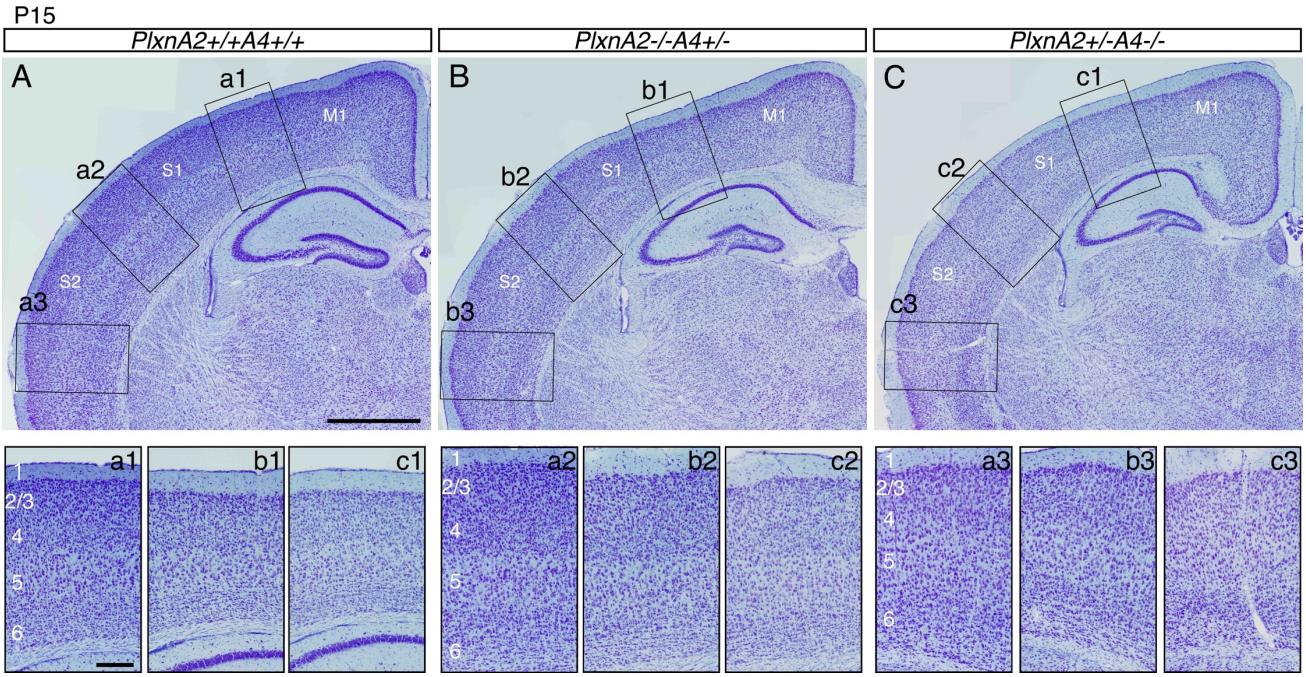

Figure S1. Cortical cytoarchitecture of *PlxnA2/A4* compound mutant mice, related to Figure 1

(A–C) Nissl staining of coronal sections from wild-type (A, *PlxnA2*$^{+/+}$*A4*$^{+/+}$) and combined single heterozygous with single homozygous mutant (B, *PlxnA2*$^{-/-}$*A4*$^{+/-}$; C, *PlxnA2*$^{+/-}$*A4*$^{-/-}$) mice at P15. Lower panels: higher-magnification views of dorsal (a1, b1, c1), dorsolateral (a2, b2, c2), and lateral (a3, b3, c3) regions of the sections in A, B, and C. These mice showed a clear L1–L2/3 boundary, indicating that PlxnA2 and PlxnA4 compensate for each other in suppressing ectopic neuronal localization in L1.
Scale bars: 1 mm in (A–C); 200 μm in (a1–c3).

Figure S2

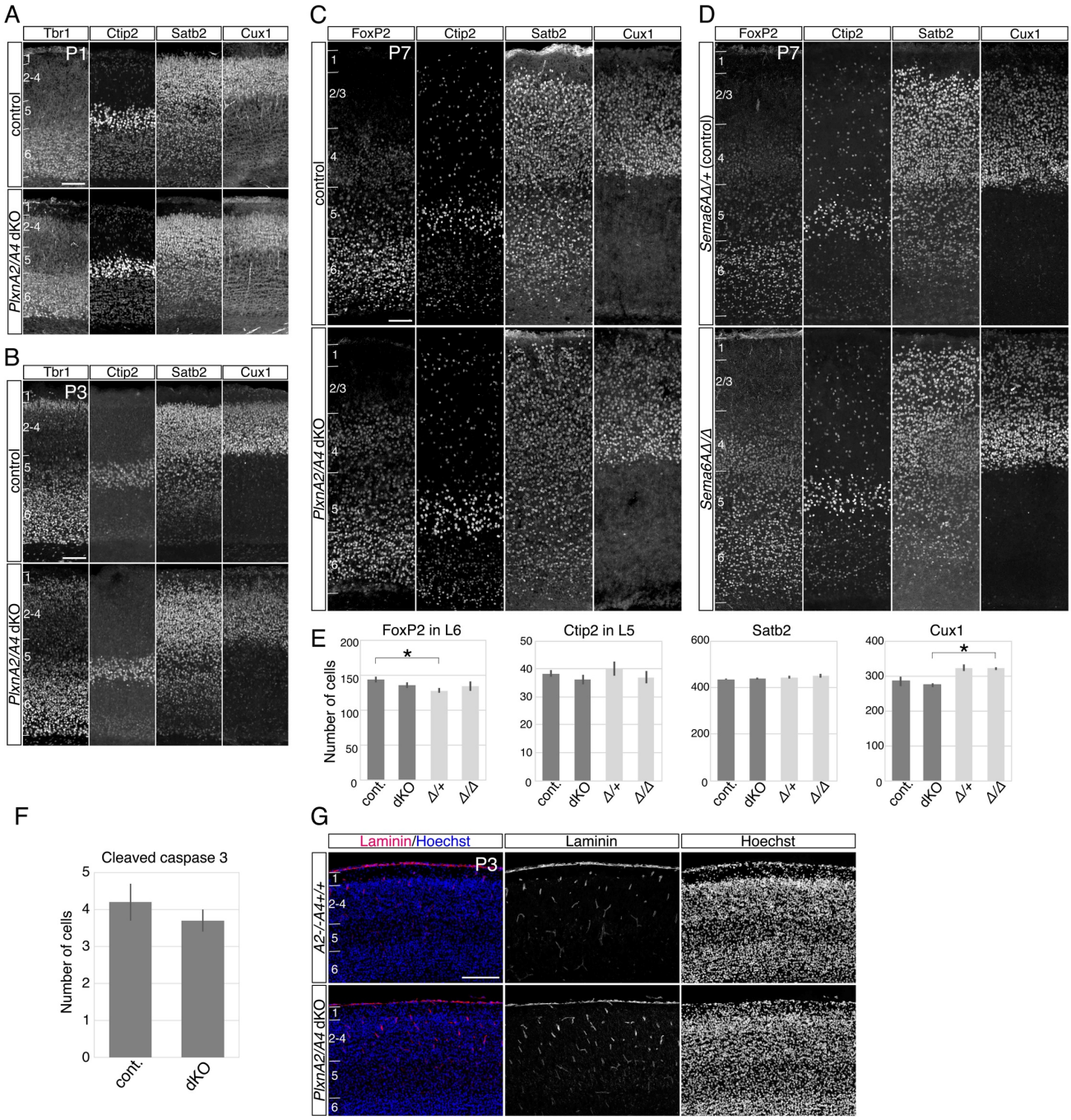

Figure S2. Cortical cell structure of *PlxnA2/A4* dKO mice and *Sema6A*$^{\Delta/\Delta}$ mice at early postnatal stages, related to Figures 2 and 6.

(A–C) Immunostaining of coronal sections from control and *PlxnA2/A4* dKO mice taken from early postnatal stages (P1, P3, and P7) using cortical layer markers. There was no apparent difference in cellular position between control and *PlxnA2/A4* dKO mice except for the superficial region, supporting the notion that the migration and

termination of deeper layer neurons do not depend on Sema6A–PlxnA2/A4 signaling.
(D) Immunostaining of coronal sections from control *Sema6A*$^{\Delta/+}$ and *Sema6A*$^{\Delta/\Delta}$ mice at P7 using cortical layer markers.
(E) Bar histogram showing the number of layer marker-positive cells located within a width of 100 μm in the S1 area of *PlxnA2/A4* dKO and *Sema6A*$^{\Delta/\Delta}$ mice at P7. Three or four regions from each genotype were examined. Data are represented as mean ± SEM. Although there was a slight difference between *PlxnA2/A4* dKO and *Sema6A*$^{\Delta/\Delta}$ mouse lines, no significant difference was found between any pair of control and corresponding gene mutants. *$p < 0.05$ (one-way ANOVA followed by Tukey's *post-hoc* test).
(F) Bar histogram showing the number of cleaved caspase-positive cells in a 600 μm-wide cerebral wall strip of lateral cortex at P1. Control (4.2 ± 0.5, $n = 30$ strips of right and left hemispheres from 2 brains) and *PlxnA2/A4* dKO mice (3.7 ± 0.3, $n = 30$ strips as described above). Data are represented as mean ± SEM. No significant difference was found (Student's t-test).
(G) Laminin staining of coronal sections from control (*PlxnA2*$^{-/-}$*A4*$^{+/+}$) and *PlxnA2/A4* dKO mice at P3. No abnormality of the glia limiting membrane was observed in regions where ectopic L1 cells were present.
Scale bars: 200 μm in (G); 100 μm in (A), (B), and (C and D).

Figure S3

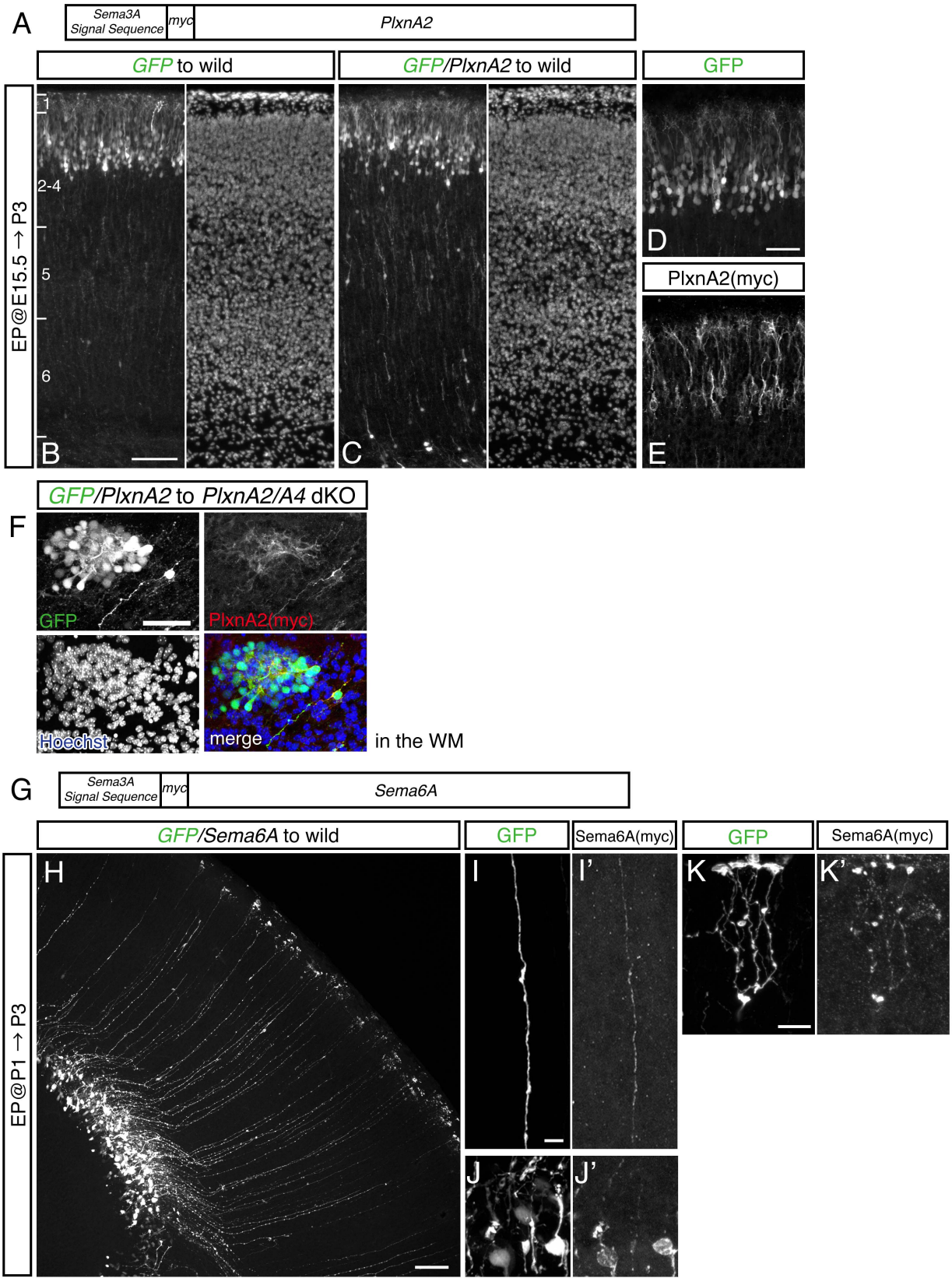
A
Sema3A Signal Sequence
myc
PlxnA2
GFP to wild
GFP/PlxnA2 to wild
GFP
EP@E15.5 → P3
1
2-4
5
6
B
C
D
PlxnA2(myc)
E
F
GFP/PlxnA2 to PlxnA2/A4 dKO
GFP
PlxnA2(myc)
Hoechst
merge
in the WM
G
Sema3A Signal Sequence
myc
Sema6A
GFP/Sema6A to wild
GFP
Sema6A(myc)
GFP
Sema6A(myc)
EP@P1 → P3
H
I
I'
K
K'
J
J'

Figure S3. Transfection of *PlxnA2* in SLN progenitors and of *Sema6A* in VZ cells, related to Figures 5 and 6.

(A) Construction of *myc*-tagged *PlxnA2* in an expression vector.

(B and C) *GFP* alone (B) or a mixture of *GFP* and *myc*-tagged *PlxnA2* (C) plasmids was introduced into prospective SLNs of wild-type mice at E15.5 by IUE. Sections were examined at P3. Right panels are nuclear staining. No gross abnormalities were found in the position of GFP^+ neurons with supplemented PlxnA2 expression in wild-type mice.

(D and E) Higher-magnification views of GFP and PlxnA2 (visualized by anti-myc staining) after transfection with *GFP/PlxnA2*. Exogenous PlxnA2 was localized on the cell surface, particularly on immature apical processes and their arbors, supporting the notion that PlxnA2 functions in the leading processes of SLNs.

(F) GFP/PlxnA2-$high^+$ cells aggregated in the WM of *PlxnA2/A4* dKO mice. Cells exhibiting high expression of GFP/PlxnA2 (judged from strong GFP fluorescence and myc immunoreactivity) in dKO mice often formed large cell aggregates in the WM and did not enter the CP. They tended to adhere to each other through their leading processes. Aggregates appeared to be composed only of GFP/$PlxnA2^+$ cells.

(G) Construction of *myc*-tagged *Sema6A* in an expression vector.

(H–K') A mixture of *GFP* and *myc*-tagged *Sema6A* plasmids was introduced into VZ cells of wild-type mice at P1 by electroporation and sections were examined at P3. High-magnification views of GFP and Sema6A-electroporated cell processes (visualized by anti-myc staining) in the VZ (J, J'), the CP (I, I'), and L1 (K, K').

Scale bars: 100 μm in (B and C) and (H); 50 μm in (D and E) and (F); 10 μm in (I–J') and (K and K').

Figure S4

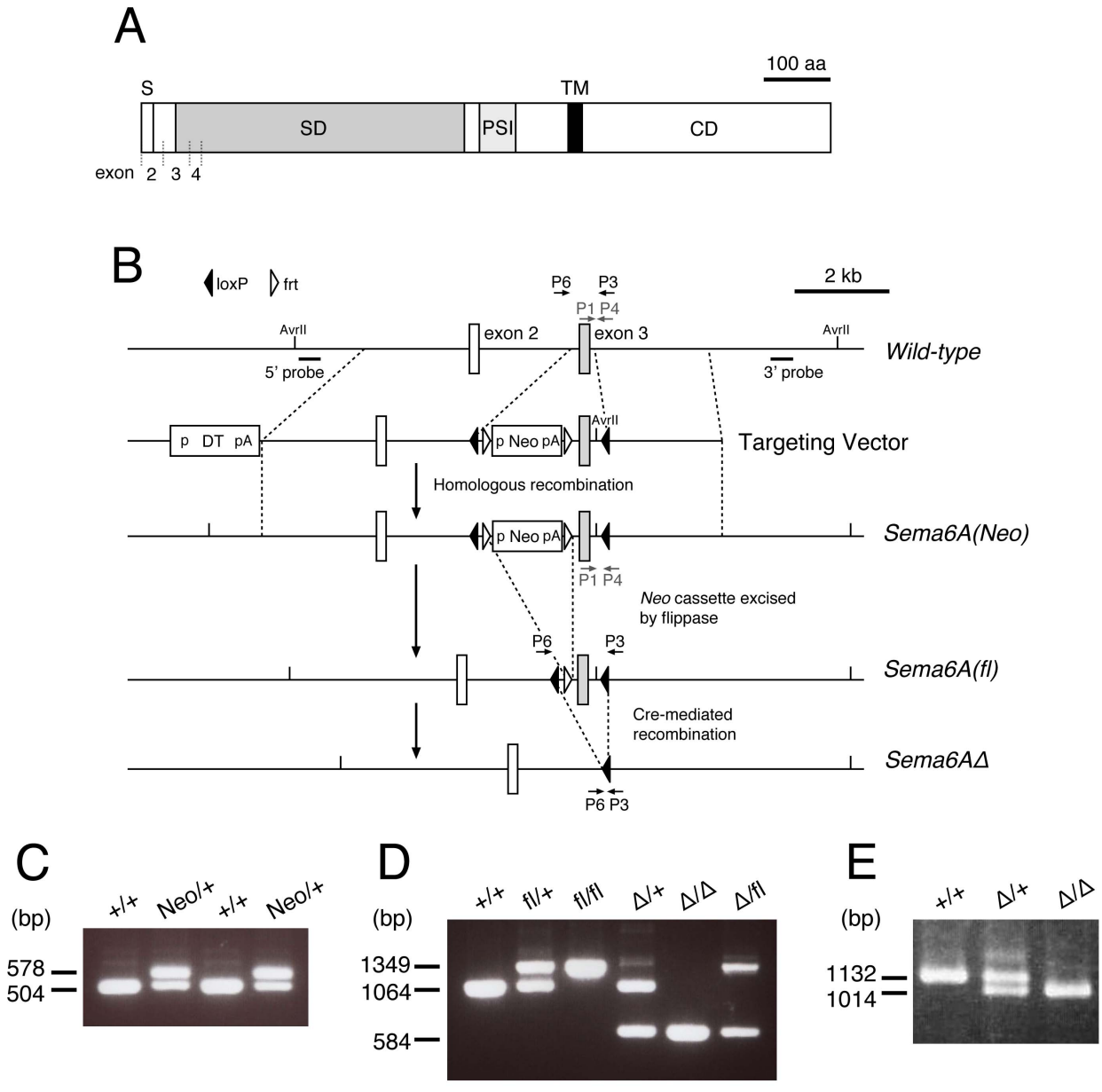

Figure S4. Generation of *Sema6A*-floxed and -deleted mice, related to Figures 6 and 7.

(A) Location of the targeted exon 3 in Sema6A protein. All reported mRNA splicing variants for *Sema6A* include exons 2, 3, and 4 (adapted from NM_018744). Exon 2 (138 bp) includes the ATG translation initiation codon and signal peptide (S). Exons 3 (118 bp) and 4 (61 bp) encode the amino-terminal region of the sema domain (SD), which is essential for semaphorin signaling. We targeted exon 3 for generating *Sema6A*-floxed

and -deleted mice because removal of exon 2 might produce a *Sema6A* transcript that contains a new in-frame ATG codon from exon 3, which would produce almost an entire Sema6A protein except for the signal peptide. On the other hand, removal of exon 3 could delete the sema domain and provide premature termination codons in the following exon 4. PSI: the plexin-semaphorin-integrin domain; TM: transmembrane domain; CD: cytoplasmic domain.
(B) Targeting strategy for production of *Sem6A*-floxed and -deleted mice. Exon 3 of the wild-type *Sema6A* locus was targeted by homologous recombination with a gene construct containing an insertion of the neomycin resistance cassette (*Neo*) flanked by *frt* sites (white arrowheads) with *loxP* sites (black arrowheads) upstream and downstream of exon 3, and the diphtheria toxin A fragment gene cassette (DT) at the 5' flank of the construct. The targeted allele was designated as *Sema6A*(*Neo*). Homologous recombinant ES clones were identified by Southern blot analysis with probes for 5' and 3' regions.
(C) PCR analysis for heterozygous offspring having the *Sema6A*(*Neo*) allele. Wild-type and *Sema6A*(*Neo*) allele yielded 504-bp and 578-bp products, respectively, with P1 (5'-CCGGTGTTTGTGGGCCACAAG-3') and P4 (5'-CTATAATAGACACACATCTCTGCCC-3') primers.
(D) PCR analysis for wild-type, *Sema6A*-floxed [*Sema6A*(*fl*)], and *Sema6A*-deletion [*Sema6AΔ*] alleles. The *Sema6A*(*fl*) allele was generated by removing the *Neo* cassette in the *Sema6A*(*Neo*) allele by mating heterozygous mice with ROSA26::FLPe Knock-in mice (RRID:MGI5438838). The *Sema6AΔ* allele was generated by removing exon 3 in the *Sema6A*(*fl*) allele by mating with CAG-Cre mice. Wild-type, *Sema6A*(*fl*), and *Sema6AΔ* alleles yielded 1064-, 1349-, and 584-bp products, respectively, with P6 (5'-GCCAATTGCTTAGCTCCAGTGTG-3') and P3 (5'-GACAGTTGTTTGTTAAACCGACTTG-3') primers.
(E) RT-PCR analysis of *Sema6A* mRNA in a *Sema6AΔ* mouse. *Sema6A* transcripts from wild-type and *Sema6AΔ* mutant embryos yielded 1132- and 1014-bp products, respectively, with F1 (5'-GAGAAGCAAGTCCCCCCGCTGAACC-3', in exon 2) and R4 (5'-CAGCCTGGCCTGGGCTTAGGGACTC-3', in exons 11 and 12) primers. Sequence analysis of these PCR products showed that exon 3 was indeed deleted in the mutant transcript, confirming no production of functional Sema6A protein. Note that homozygous *Sema6AΔ* allele mice (*Sema6A*$^{\Delta/\Delta}$) and *Sema6A* gene trap mutant mice (*Sema6A*$^{-/-}$) apparently showed the same defects, including malformations in the cortical laminar structure (this study), and projection of olfactory bulb axons and thalamocortical axons (data not shown). These characteristics further support the notion that the *Sema6AΔ* allele is functionally null. In contrast, homozygous *Sema6A*(*fl*) allele mice (*Sema6A*$^{fl/fl}$) had no obvious defect, indicating that this allele is functional.

Figure S5

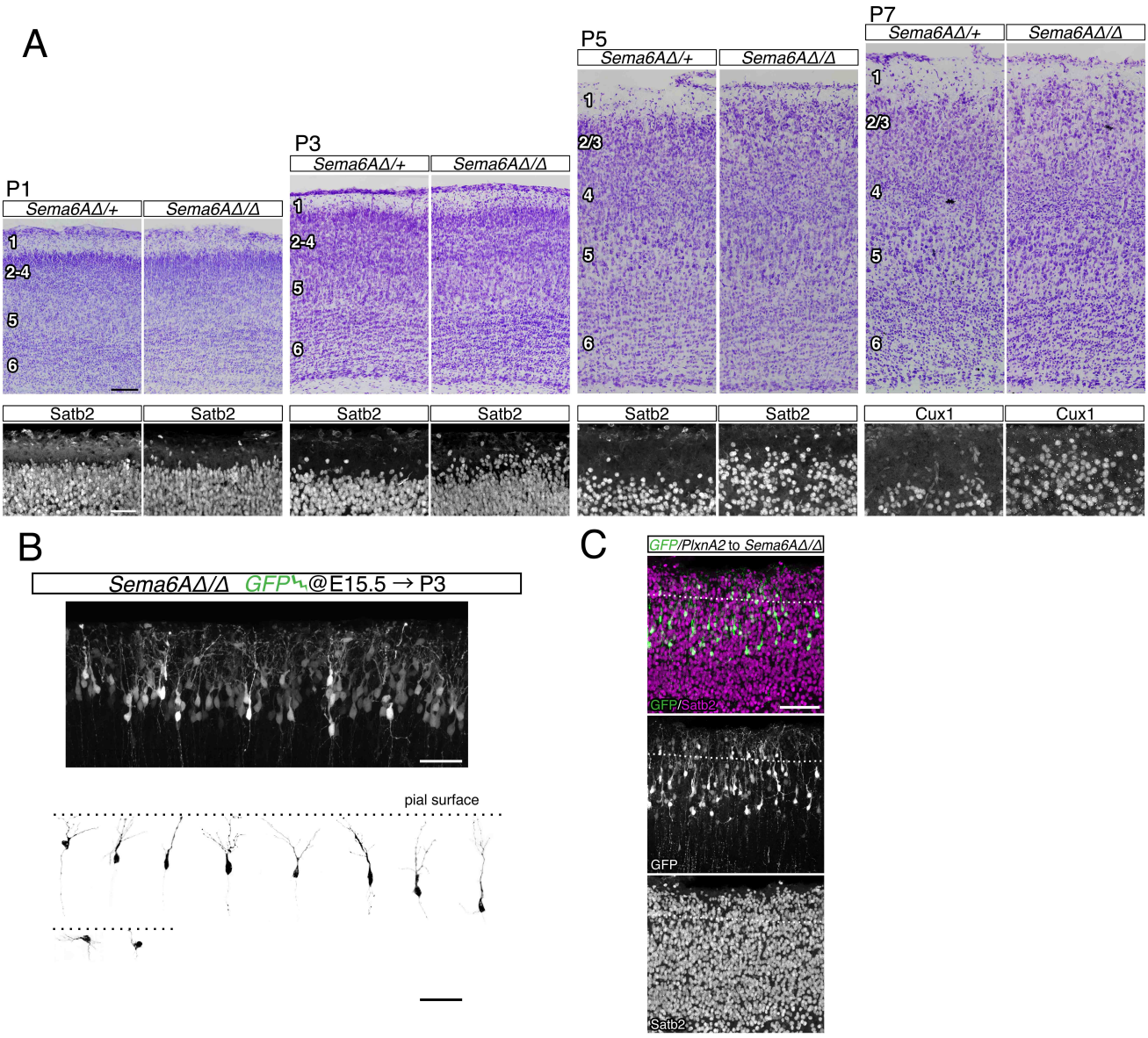

Figure S5. SLN mislocation in *Sema6A*$^{\Delta/\Delta}$ mice at early postnatal stages, related to Figures 2, 3 and 6.

(A) Nissl staining (upper panels) and immunostaining (lower panels) of the presumptive primary somatosensory area of *Sema6A*$^{\Delta/+}$ and *Sema6A*$^{\Delta/\Delta}$ mice at P1, P3, P5, and P7. Satb2 staining showed that disorganization of SLNs was manifested at around P3. The Satb2 malpositioning seemed to occur in a low-medial-to-high-lateral gradient manner. The irregular neuronal clusters (not included here), which were also observed in *PlxnA2/A4* dKO mice, were first recognized at P5 in the lateral region of *Sema6AΔ/Δ* mice. While all animals had neuronal clusters, individuals varied regarding the appearance frequency.

(B) Upper panel: SLNs observed at the time of their migration termination. GFP^+ SLNs labeled at E15.5 of *Sema6A*$^{\Delta/\Delta}$ mice reached their target layer by P3. Lower panel: 3D reconstruction images of GFP^+ SLNs. The dotted line indicates the position of the pial surface. See also Figure 3J to compare with GFP^+ SLNs of *PlxnA2/A4* dKO mice. Apical processes of SLNs in both *Sema6A*$^{\Delta/\Delta}$ and *PlxnA2/A4* dKO mice tended to be shorter than those in control mice.
(C) Transfection of a mixture of *GFP* and *PlxnA2* plasmids into SLN progenitors of *Sema6A*$^{\Delta/\Delta}$ mice, by IUE at E15.5; the brain was examined at P3. Top: merged views of GFP fluorescence and Satb2 staining. Middle and bottom: GFP and Satb2 views, respectively.
Scale bars: 100 μm in (A, upper panels) and (C); 50 μm in (A, lower panels) and (B, upper and lower panels).

Figure S6

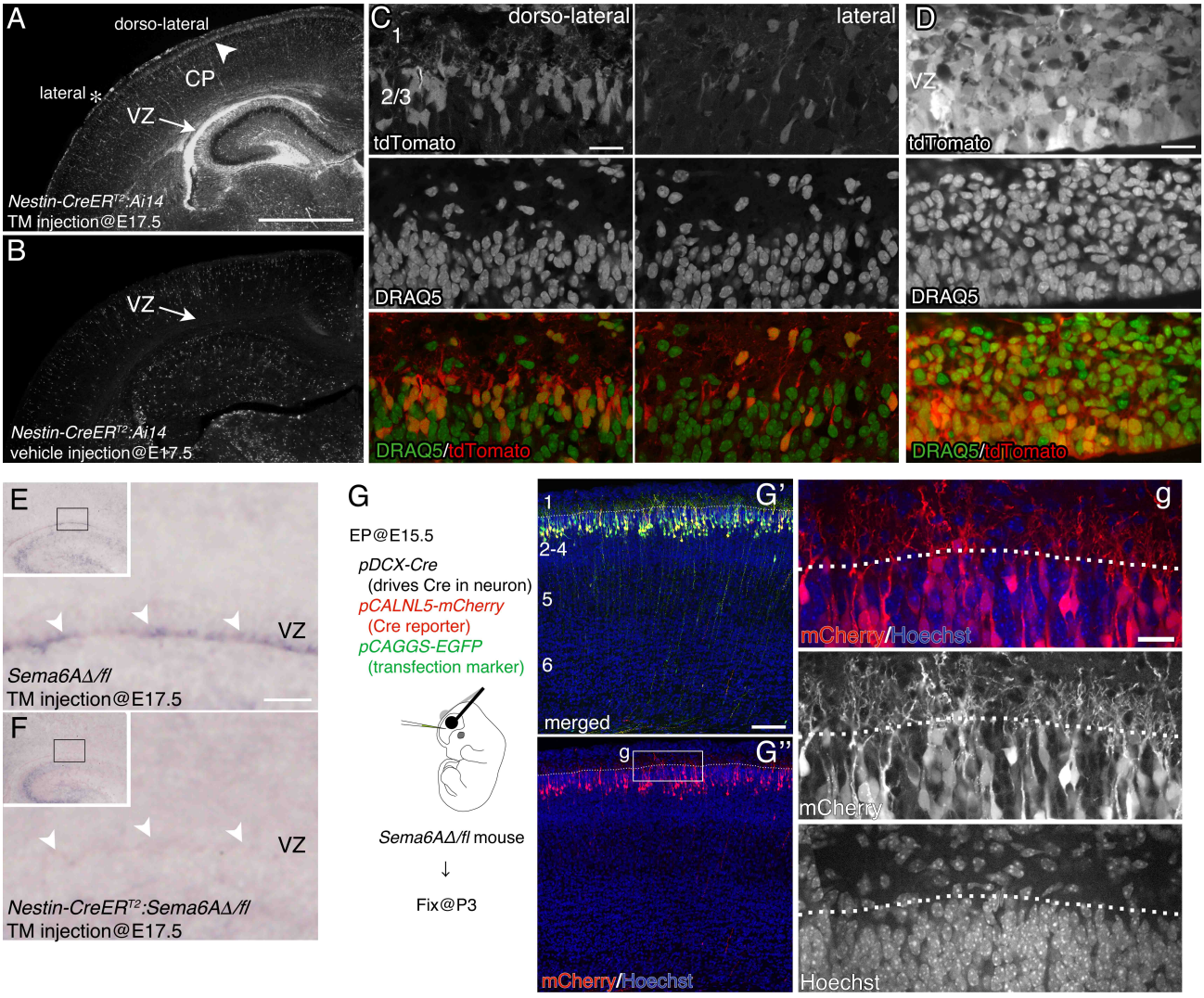

Figure S6. Targeted recombination in VZ cells at the perinatal stage by administration of tamoxifen to *Nestin-CreER^{T2}* mice, related to Figure 7.

(A and B) *NestinCreER^{T2}:Ai14* mice were injected with tamoxifen (A) or only corn oil (B) at E17.5 and fixed at P3. Gene recombination was mainly observed in VZ cells (arrows). It also occurred in a small fraction of SLNs in the dorsolateral region (arrowhead), but hardly at all in the lateral region (asterisk), based on a neurogenetic gradient (Bayer and Altman, 1991).

(C) Higher-magnification views of SLNs in the dorsolateral and lateral regions. Note that after administration of tamoxifen to *NestinCreER^{T2}:Sema6A* mice (Figure 7), ectopic neurons in L1 occurred in a dorsal-low and lateral-high pattern, consistent with the notion that their phenotypes were independent of the *Sema6A* inactivation in SLNs.

(D) Higher-magnification views of cells in the VZ. Recombination occurred for the

majority of VZ cells.
(E and F) *In situ* hybridization signals of a Sema6A-exon 3 probe on sections taken from *Sema6A*$^{\Delta/fl}$ (E) and *NestinCreER*^{T2}*:Sema6A*$^{\Delta/fl}$ (F) littermates, injected with tamoxifen at E17.5 and fixed at P3. Signals in VZ cells (arrowheads) were diminished in the mouse carrying the *NestinCreER*^{T2} gene.
(G) A mixture of *pDCX-Cre*, *pCALNL5-mCherry* (floxed *mCherry*), and *pCAGGS-EGFP* plasmids was transfected into progenitors of SLNs of a *Sema6A*$^{\Delta/fl}$ mouse by IUE at E15.5 and examined at P3. Blue indicates nuclear counterstain. (G') Merged views of mCherry/EGFP/Hoechst fluorescence and (G") mCherry/Hoechst fluorescence. Dotted lines indicate the L1–L2/3 boundary. The white rectangle (g) is enlarged in the right three panels. No mCherry^{+} cells were found in L1.
Scale bars: 1 mm in (A and B); 20 μm in (C), (D), and (g); 50 μm in (E and F) and (G).

Figure S7

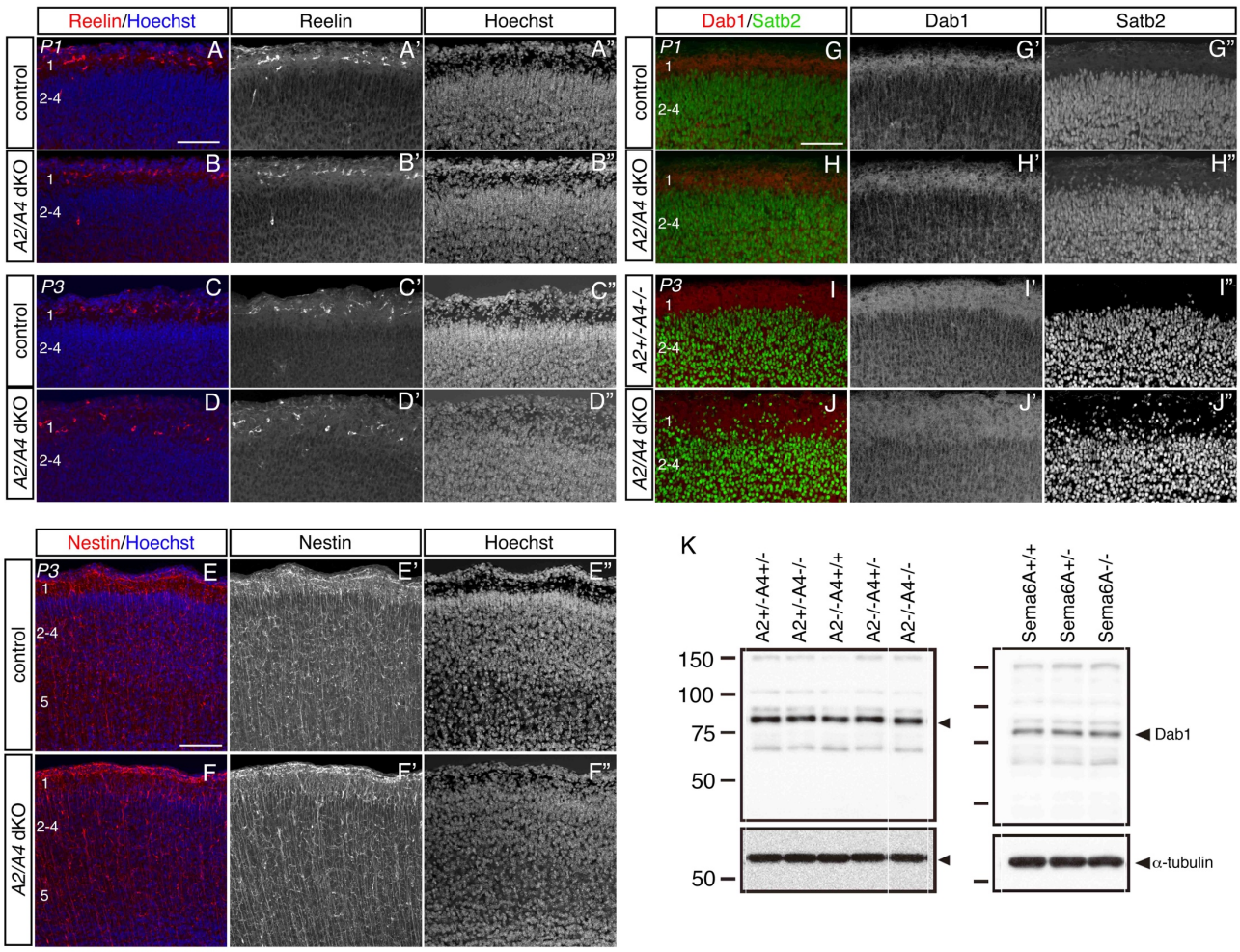

Figure S7. No apparent changes in reelin-related signaling, related to Figures 1 and 6.

(A–D") Distribution of Reelin-positive Cajal-Retzius cells. Reelin was recognized by immunostaining. Control (A–A" and C–C") and *PlxnA2/A4* dKO (B–B" and D–D") mice at P1 (A–B") and P3 (C–D").

(E–F") Nestin-positive RG fibers with nuclear staining at P3.

(G–J") Expression profiles of Dab1 with Satb2 on sections from control (G–G" and I–I") and *PlxnA2/A4* dKO mice (H–H" and J–J") at P1 (G–H") and P3 (I–J").

(K) Western blot of Dab1 expression in *PlxnA2* and *A4* compound mutant (left panel) and *Sema6A*$^{-/-}$ mice (right panel). Homogenates of P3 cerebral cortices were analyzed. Anti-α-tubulin was used as a loading control. Note that sample homogenates in the left panel were all analyzed together; the panel has gaps because some lanes were removed to eliminate redundancy. No apparent change of Dab1 expression was found among these genotypes.

Scale bars: 100 μm in (A–D"), (E–F"), and (G–J").

Transparent Methods

Experimental animals

PlexinA2 (*PlxnA2*)-deleted (RRID:MGI:3795748, Suto et al., 2007), *PlxnA4*-deleted (RRID:MGI:3795749, Suto et al., 2005), *Semaphorin 6A* (*Sema6A*)-floxed [*Sema6A(fl)*; Accession No. CDB1024K: http://www2.clst.riken.jp/arg/mutant%20mice%20list.html, generated as described at http://www2.clst.riken.jp/arg/methods.html, see also Figure S4], *Sema6A*-deleted [*Sema6AΔ*; exon 3 deletion, generated by crossing *Sema6A(fl)* with CAG-Cre mice (RRID:IMSR_RBRC09807, Sakai and Miyazaki, 1997)], *Sema6A* gene trap (RRID:MGI:3037891, Leighton et al., 2001; referred to as $Sema6A^{-/-}$ to distinguish them from $Sema6A^{\Delta/\Delta}$), *Sema6B*-deleted (RRID:MGI:4461290, Tawarayama et al., 2010), *Emx1-Cre* (*Emx1-Cre*(*KΔN*), RRID:IMSR_RBRC01345, Iwasato et al., 2008), $Nestin\text{-}CreER^{T2}$ (RRID:IMSR_RBRC05999, Imayoshi et al., 2006), and *Ai14* (RRID:IMSR_JAX:007914, Madisen et al., 2010) mice were maintained in the C57BL/6 background. *PlxnA2* and *PlxnA4* double-knockout ($PlxnA2^{-/-}A4^{-/-}$; *PlxnA2/A4* dKO) mice were generated mostly by crossing $PlxnA2^{-/-}A4^{+/-}$ males, but occasionally double-heterozygous ($PlxnA2^{+/-}A4^{+/-}$) males, with either $PlxnA2^{-/-}A4^{+/-}$ or $PlxnA2^{+/-}A4^{+/-}$ females. Conditional knockout mice were prepared by crossing $Sema6A^{fl/+}$ mice with $Emx1\text{-}Cre{:}Sema6A^{\Delta/+}$ or $Nestin\text{-}CreER^{T2}{:}Sema6A^{\Delta/+}$ mice. Noon of the day of vaginal plug observation was defined as embryonic day 0 (E0). Birth usually occurs at E19 and sometimes at E20, and was designated as postnatal day (P) 0. However, in the rescue experiment (see below), pups 7 days after surgery at E15 were regarded as P3 even when their birth was delayed or effected via Caesarean section. Timed-pregnant wild-type C57BL/6 and foster ICR mice were purchased from Japan SLC (Hamamatsu). For all experiments, both male and female littermates were randomly assigned to experimental groups. E15.5 and E17.5 mouse embryos

obtained from timed-pregnant females were used for experiments of electroporation and tamoxifen administration, respectively. For analyses of the cortical structure, P1-P15 mouse pups were used. All experiments were conducted in compliance with the guidelines for use of laboratory animals of the National Institute of Genetics, the National Institute for Physiological Sciences, Osaka University and RIKEN Kobe Campus.

Tamoxifen administration

Pregnant dams received a single dose of tamoxifen (3.0 mg, Sigma-Aldrich, Cat# T5648), dissolved in corn oil (10 mg/ml), at E17.5 by intraperitoneal injection. Pups were rescued by Caesarean section on E19.5 and fostered to an ICR mother.

Immunohistochemistry

Heads of E15.5 embryos were immersion-fixed in 4% paraformaldehyde (PFA) in phosphate-buffered saline, pH 7.4 (PBS), and postnatal brains were fixed by intracardial perfusion with PBS followed by 4% PFA/PBS under deep sodium pentobarbital anesthesia (>100 mg/kg). For GABA immunostaining, intracardial perfusion was carried out with pre-fixative (8.5% w/v sucrose/5 mM $MgCl_2$/20 mM phosphate buffer, pH 7.4), followed by 4% PFA/0.2% picric acid/1% glutaraldehyde/0.1 M phosphate buffer (PB), pH 7.4. Fixed samples were stored overnight in each fixative at 4°C. For immunohistochemistry for PlxnA2 and PlxnA4, samples were fixed by perfusion and post-fixed with 2% PFA/PBS for 4 h. Brains were then cryoprotected in 30% sucrose/PBS overnight at 4°C and embedded in compound (FSC22, Leica). Frozen sections for immunohistochemistry were cut coronally with a cryostat at 30 μm and collected in PBS, or at 10–16 μm, and collected onto adhesive silane (MAS)-coated glass slides (Matsunami). For immunohistochemistry for PlxnA2 and PlxnA4 after

electroporation, fixed brains were directly cut coronally with a vibrating blade microtome (VT1000S, Leica) at 100 μm and collected in PBS. They were blocked in PBS containing 5% normal goat serum and 0.3% Triton X-100 and incubated over one or two nights at 4°C with primary antibodies. Primary antibodies used are as follows: mouse anti-α-tubulin (1:6000, Sigma-Aldrich Cat# T9026; RRID:AB_477593), rat anti-BrdU (2 μg/ml, Abcam Cat# ab6326; RRID:AB_305426), rabbit anti-cleaved caspase-3 (Asp175) (1:400, Cell Signaling Technology Cat# 9661; RRID:AB_2341188), rat anti-Ctip2 (0.5 μg/ml, Abcam Cat# ab18465; RRID:AB_10015215), rabbit anti-Cux1 (1 μg/ml, Santa Cruz Cat# sc-13024; RRID:AB_2261231), rabbit anti-Dab1 (1:2000, Uchida et al., 2009), rabbit anti-ER81 (1:6000, Covance Research Produts Cat# PRB-362C-100; RRID:AB_509963), rabbit anti-FoxP2 (1 μg/ml, Abcam Cat# ab16046; RRID:AB_2107107), rabbit anti-GABA (0.5 μg/ml, Sigma-Aldrich Cat#A2052; RRID:AB_477652), chick anti-GFP (1 μg/ml, Abcam Cat#ab13970; RRID:AB_300798), rabbit anti-laminin (1:1000, Sigma-Aldrich Cat# L9393; RRID: AB_477163), rabbit anti-myc (1:1000, Cell Signaling Cat# 2272; RRID: AB_331667), rabbit anti-nestin (1:500, Arimatsu et al., 1999), mouse anti-NeuN (1 μg/ml, Millipore Cat# mAbA60; RRID:AB_2314891), Armenian hamster anti-PlxnA2 (1:5, A2D3, Suto et al., 2007) and anti-PlxnA4 (1:5, A4F5, Suto et al., 2007), mouse anti-reelin (1:50, CR50, Ogawa et al., 1995), mouse anti-Satb2 (0.5 μg/ml, Cosmo Bio Cat# CBX-CBX00263; RRID:AB_1962472), rabbit anti-Tbr1 (3.6 μg/ml, Millipore Cat# AB9616; RRID:AB_2200223 or 2 μg/ml, Abcam Cat# ab31940; RRID:AB_2200219), and rabbit anti-Wfs1 (0.5 μg/ml, Proteintech Group Cat# 11558-1-AP; RRID:AB_2216046). Anti-IgG conjugated to biotin (1:1000), AlexaFluor488, 594 (1:1000), Cy3 (1:500), or DyLight 488 (1:400), or anti-IgY conjugated to AlexaFluor488 antibodies was used as a secondary antibody. Biotin was detected by ABC elite kit (Vector Laboratories). After these treatments, floating sections were collected onto MAS-coated glass slides.

Sections were treated with Hoechst 33342 (1 μg/μl, Dojindo) or DRAQ5 (5 μg/μl, Cell Signaling) for nuclear staining. They were mounted with Mowiol mounting medium (0.1 M Tris-HCl, pH 8.5, 25% glycerol, 10% Mowiol 4-88 Reagent, Calbiochem; and 2.5% 1,4-diazabicyclo-[2.2.2]-octan, Sigma-Aldrich) for fluorescence immunohistochemistry or with Entellan new (Merck) for other histochemistry. The sections were examined with Axioplan2 coupled to an AxioCam HRm camera (Zeiss) or BX60 coupled to a DP73 camera (Olympus). Z-series confocal images (FV1000, Olympus; LSM510Meta, LSM710 and LSM780, Zeiss; A1R, Nikon) of sections were captured and assembled into a single image by Fiji software (Schindelin et al., 2012) or ZEN microscope software (Zeiss). All images were imported into Adobe Photoshop CS5.1, and montages of images were constructed after minor contrast and brightness adjustment.

In situ *hybridization*

Frozen sections were cut with a cryostat at 16 μm and collected onto MAS-coated glass slides. Antisense riboprobes labeled with digoxigenin-11-UTP (DIG, Roche) were generated by *in vitro* transcription of cDNA encoding *PlxnA2* (1.0 kbp, Murakami et al., 2001), *PlxnA4* (0.7 kbp, Suto et al., 2003), *Sema6A* (0.5 kbp, Suto et al., 2005), or *Sema6A-exon 3* (118 bp, we used forward primer: ATACAAAACAGTATCCGGTG, and reverse primer: TAATACGACTCACTATAGGGCGAGCAGCAACGTAGAGG that contains T7 promoter to make the template). *In situ* hybridization was performed as described previously with some modifications (Hatanaka and Jones, 1998). In brief, DIG-labeled probes were dissolved in 50% formamide, 5x SSC, 1% SDS, 50 μg/ml heparin, and 50 μg/ml yeast RNA, and hybridized overnight at 65°C. Following hybridization, sections were washed, treated with RNaseA (20 μg/ml, 37°C, 10 min),

and incubated with alkaline phosphatase-conjugated anti-DIG antibody (1:1,000) overnight at 4°C. Color reaction was carried out for 2-3 days at room temperature in BM purple (Roche). Sections were mounted with Aqua-Poly/Mount (Polysciences).

BrdU labeling

Mouse embryos were intraperitoneally injected with 5-bromo-2-deoxyuridine (BrdU; Sigma-Aldrich; 50 mg/kg body weight) at E15.5 or E16.5 and were fixed at P7. Free-floating brain sections were pre-incubated in 2 N HCl for 60 min at 37°C before fluorescence immunohistochemistry. Images of the S1 area in coronal sections were captured under a confocal microscope. For quantification, the cerebral wall was divided into 10 equal bins (bin 1–10) from the bottom of layer 6 to the pial surface (see Figure 3), and the numbers of $BrdU^+$ cells in each bin were counted manually. We counted 944, 833, and 731 cells in three E15.5 control mice, and 696, 660, and 733 cells in three dKO mice; 322, 275, and 519 cells in three E16.5 control mice and 408, 251, and 369 cells in dKO mice.

Electroporation

EGFP (Hatanaka et al., 2004), *myc-PlxnA2* (Figure S3A, Murakami et al., 2001), and *myc-Sema6A* (Figure S3G, Suto et al., 2007) cloned into *pCAGGS* (Niwa et al., 1991), *mCherry* cloned into *pCALNL5* (Hatanaka and Yamauchi, 2013), and *nCre* cloned into *pDCX* (this vector was made by replacing the *CAG* promoter in *pCAGGS* with the *DCX* promoter, Franco et al., 2011) were used. *pCAGGS-EGFP* at a final concentration of 1 μg/μl was used for location and morphological examination of cortical neurons in control and *PlxnA2/A4* dKO mice. For rescue experiments, we used a mixture of *pCAGGS-myc-PlxnA2* (2 μg/μl) and *pCAGGS-EGFP* (1 μg/μl); for *Sema6A* conditional knockout, a mixture of *pDCX-nCre* (0.5 μg/μl), *pCALNL5-*

mCherry (1 μg/μl), and *pCAGGS-EGFP* (1 μg/μl); and for exogenous Sema6A expression, a mixture of *pCAGGS-myc-Sema6A* (5 μg/μl) and *pCAGGS-EGFP* (1 μg/μl). Plasmids were prepared using an EndoFree Plasmid Maxi Kit (Qiagen). Fast Green (final concentration: 0.025%) was added to monitor the injection. *In utero* electroporation was carried out basically as described previously (Hatanaka and Yamauchi, 2013), except that we reduced the number of electric pulses from five to four and used 3-mm round plate forceps-shaped electrodes (CUY650P3, Nepagene). Occasionally, pups were delivered by Caesarean section, and raised to P3 by an ICR foster mother. Electroporation for postnatal pups (P1) was performed as described previously with some modifications (Boutin et al., 2008). Briefly, after anesthesia by hypothermia, plasmids were injected into the lateral ventricle through the skull with a pulled glass capillary. Five-millimeter-diameter round plate forceps-shaped electrodes (CUY650P5) coated with a small amount of PBS were placed on the top of the head and under the jaw, and four electric pulses were delivered (80 V, 50-ms pulse length, 950-ms intervals). Pups were then placed at 37°C for warming before being returned to their mother, and allowed to develop to P3.

For morphological examination, 30-μm-thick sections were treated with an anti-GFP antibody. Z-series of images of GFP cells in sparsely labeled regions were captured by confocal laser scanning microscopy under a 60x objective and traced manually.

For quantitation of rescue experiments, counting was performed on three images in each sample with a width of 450 μm of presumptive S1 area, which was identified by its location and thick upper layers recognized by the distribution of $Satb2^+$ cells, at the level of the rostral part of the hippocampus. The percentage of GFP^+ cells in L1 at P3 was calculated from the total number of GFP^+ cells observed in the CP and L1. A fraction of neurons that showed high PlxnA2 expression formed

aggregates in the white matter. These were excluded from the calculation (see Results). Statistical analysis (Excel and GraphPad Prism software, version 4.0) was done using one-way ANOVA followed by Tukey's *post-hoc* test. Statistical significance was defined at $*p < 0.05$.

Quantitation of the number of Satb2-positive neurons in L1

The number of GFP^+ or $Satb2^+$ cells located in L1 (within 70 μm from the pia matter) was counted on three images in each genotype or in manipulated mice as described above. The position of the L1–L2/3 boundary was also monitored by Hoechst 33342 staining. Statistical analysis was as described above.

Western blot of Dab1 protein

Cortical lobes were excised from P3 mice and homogenized in lysis buffer (50 mM Tris-HCl, pH 8.0, 150 mM NaCl, 5 mM EDTA, 1% Triton X-100, 0.1% sodium deoxycholate, 10 mM Na_3VO_4). Total protein concentration was determined using the BCA Protein Assay Kit (Thermo Fisher Scientific). Equal aliquots of protein (10 μg) were analyzed by SDS-PAGE, followed by western blotting using anti-Dab1 (1:2000, Uchida et al., 2009) and anti-α-tubulin (1:6000) antibodies.

X-gal staining

P1 *Sema6A*$^{+/-}$ mouse brains were immersion-fixed in 2% PFA/0.2% picric acid/0.1 M PB for 1 h on ice, cryoprotected in 20% sucrose/PBS, and embedded in compound. Staining with 5-bromo-4-chloro-3-indolyl-ß-D-galactopyranoside (X-gal, Wako) was carried out on 8-μm frozen sections. The sections were then subjected to immunohistochemistry for Satb2, Ctip2, or reelin.

Binding assay using alkaline phosphatase (AP)-fused proteins

The procedures basically followed previously reported methods (Flanagan et al., 2000). The expression plasmids for AP-PlxnA2 (AP is fused with the sema domain of PlxnA2; Renaud et al., 2008) and AP-Sema6A (AP and Fc are fused with the extracellular domain of Sema6A; Suto et al., 2005) were transfected into HEK293T cells by lipofection with FuGENE 6 reagent (Roche, Mannheim, Germany). After 3 days in culture, the culture medium was collected, filtered, and stored at 4°C as a probe solution. P1 mouse brains were dissected out in ice-cold HBAH buffer (Hanks' solution, containing 0.5 mg/ml bovine serum albumin and 20 mM HEPES, pH 7.0) and sliced into 200-μm-thick sections using a vibrating microtome (DTK1000, Dosaka-EM, Japan). Sections were incubated in the probe solution for 90 min at 4°C, washed 5 times in HBAH buffer for 10 min each, and fixed with 4% PFA/PBS for 2 h on ice. They were then incubated in HBS buffer (150 mM NaCl, 20 mM HEPES, pH 7.0) for 2 h at 65°C to inactivate endogenous phosphatases. Heat-treated sections were rinsed once with AP staining buffer (100 mM NaCl, 5 mM $MgCl_2$, 100 mM Tris-HCl, pH 9.5) and incubated in AP staining buffer containing 2% (v/v) BCIP/NBT stock solution (Roche) at room temperature. After staining, sections were washed and kept in stop solution (PBS containing 10 mM EDTA) at room temperature. They were treated with DAPI (4',6-diamidino-2-phenylindole, 1 μg/ml, Dojindo) for nuclear staining.

Supplemental References

Arimatsu, Y., Ishida, M., Takiguchi-Hayashi, K., and Uratani, Y. (1999). Cerebral cortical specification by early potential restriction of progenitor cells and later phenotype control of postmitotic neurons. Development *126*, 629-638.

Bayer, S.A., and Altman, J. (1991). Neocortical Development (New York: Raven Press).

Boutin, C., Diestel, S., Desoeuvre, A., Tiveron, M.C., and Cremer, H. (2008). Efficient in vivo electroporation of the postnatal rodent forebrain. PLoS One *3*, e1883.

Flanagan, J.G., Cheng, H.J., Feldheim, D.A., Hattori, M., Lu, Q., and Vanderhaeghen, P. (2000). Alkaline phosphatase fusions of ligands or receptors as in situ probes for staining of cells, tissues, and embryos. Methods Enzymol. *327*, 19−35.

Hatanaka, Y., and Jones, E.G. (1998). Early region-specific gene expression during tract formation in the embryonic rat forebrain. J. Comp. Neurol. *395*, 296-309.

Hatanaka, Y., and Yamauchi, K. (2013). Excitatory cortical neurons with multipolar shape establish neuronal polarity by forming a tangentially oriented axon in the intermediate zone. Cereb. Cortex *23*, 105-113.

Madisen, L., Zwingman, T.A., Sunkin, S.M., Oh, S.W., Zariwala, H.A., Gu, H., Ng, L.L., Palmiter, R.D., Hawrylycz, M.J., Jones, A.R.*, et al.* (2010). A robust and high-throughput Cre reporting and characterization system for the whole mouse brain. Nat. Neurosci. *13*, 133-140.

Sakai, K., and Miyazaki, J. (1997). A transgenic mouse line that retains Cre recombinase activity in mature oocytes irrespective of the cre transgene transmission. Biochem. Biophys. Res. Commun. *237*, 318-324.

Schindelin, J., Arganda-Carreras, I., Frise, E., Kaynig, V., Longair, M., Pietzsch, T., Preibisch, S., Rueden, C., Saalfeld, S., Schmid, B.*, et al.* (2012). Fiji: an open-source platform for biological-image analysis. Nat Methods *9*, 676-682.

Uchida, T., Baba, A., Perez-Martinez, F.J., Hibi, T., Miyata, T., Luque, J.M., Nakajima, K., and Hattori, M. (2009). Downregulation of functional Reelin receptors in projection neurons implies that primary Reelin action occurs at early/premigratory stages. J. Neurosci. *29*, 10653-10662.